The American Journal of Pathology, Vol. 192, No. 2, February 2022

ELSEVIER

The American Journal of
PATHOLOGY

ajp.amjpathol.org

BIOMARKERS, GENOMICS, PROTEOMICS, AND GENE REGULATION

ZFP36L1 Regulates *Fgf21* mRNA Turnover and Modulates Alcoholic Hepatic Steatosis and Inflammation in Mice

Chandra S. Bathula,* Jian Chen,* Rahul Kumar,* Perry J. Blackshear,† Yogesh Saini,* and Sonika Patial*

From the Department of Comparative Biomedical Sciences, School of Veterinary Medicine, Louisiana State University, Baton Rouge, Louisiana; and the Signal Transduction Laboratory,† National Institute of Environmental Health Sciences, Research Triangle Park, North Carolina*

Accepted for publication October 29, 2021.

Address correspondence to Sonika Patial, D.V.M., Ph.D., D.A.C.V.P., Department of Comparative Biomedical Sciences, School of Veterinary Medicine, Louisiana State University, Baton Rouge, LA 70803. E-mail: spatial@lsu.edu.

Zinc finger protein 36 like 1 (ZFP36L1) enhances the turnover of mRNAs containing AU-rich elements (AREs) in their 3′-untranslated regions (3′UTR). The physiological and pathological functions of ZFP36L1 in liver, however, remain largely unknown. Liver-specific ZFP36L1-deficient (*Zfp36l1*$^{flox/flox}$/Cre^{+}; L1^{LKO}) mice were generated to investigate the role of ZFP36L1 in liver physiology and pathology. Under normal conditions, the L1^{LKO} mice and their littermate controls (*Zfp36l1*$^{flox/flox}$/Cre^{-}; L1^{FLX}) appeared normal. When fed a Lieber-DeCarli liquid diet containing alcohol, L1^{LKO} mice were significantly protected from developing alcohol-induced hepatic steatosis, injury, and inflammation compared with L1^{FLX} mice. Most importantly, fibroblast growth factor 21 (*Fgf21*) mRNA was significantly increased in the livers of alcohol diet–fed L1^{LKO} mice compared with the alcohol diet–fed L1^{FLX} group. The *Fgf21* mRNA contains three AREs in its 3′UTR, and *Fgf21* 3′UTR was directly regulated by ZFP36L1 in luciferase reporter assays. Steady-state levels of *Fgf21* mRNA were significantly decreased by wild-type ZFP36L1, but not by a non-binding zinc finger ZFP36L1 mutant. Finally, wild-type ZFP36L1, but not the ZFP36L1 mutant, bound to the *Fgf21* 3′UTR ARE RNA probe. These results demonstrate that ZFP36L1 inactivation protects against alcohol-induced hepatic steatosis and liver injury and inflammation, possibly by stabilizing *Fgf21* mRNA. These findings suggest that the modulation of ZFP36L1 may be beneficial in the prevention or treatment of human alcoholic liver disease. *(Am J Pathol 2022, 192: 208–225; https://doi.org/10.1016/j.ajpath.2021.10.017)*

The mouse zinc finger protein 36 (ZFP36) family consists of four RNA binding proteins: zinc finger protein 36, alias tristetraprolin (TTP), zinc finger protein 36 like 1 (ZFP36L1), zinc finger protein 36 like 2 (ZFP36L2), and zinc finger protein 36 like 3 (ZFP36L3). All four of these proteins regulate mRNA stability by binding to AU-rich elements (AREs) within the 3′-untranslated regions (3′UTRs) of target mRNAs, resulting in ARE-mediated mRNA degradation.[1,2] Despite their common mode of biochemical action, the ZFP36 family members appear to play roles in different physiological processes. This is apparent from the fact that germline deletion of all four ZFP36 family members in mice has resulted in varied phenotypes.[3–6] ZFP36, or TTP, is the best-studied family member and plays an essential role in controlling inflammation.[7,8] However, the roles of the other three members of the ZFP36 family remain poorly understood.

Recent studies have found that ZFP36L1 is involved in the regulation of mRNAs associated with metabolic functions. For example, ZFP36L1 has been shown to post-transcriptionally regulate the levels of the low-density lipoprotein receptor, a protein that is highly expressed in the liver and is a major determinant of circulating levels of low-density lipoprotein, linking ZFP36L1 to cholesterol metabolism.[9] ZFP36L1 has also been shown to post-transcriptionally regulate uncoupling protein 1 (UCP1), which plays an important role in thermogenesis.[10] Similarly, ZFP36L1 was recently shown to regulate liver bile

Supported by Louisiana State University (LSU) COBRE (NIH/NIGMS grant # 5P30GM110760 and P20GM130555) and LSU SVM Startup funds (S.P.), and in part by the National Institute of Environmental Health Sciences, NIH, Intramural Research Program (P.J.B.).

Disclosures: None reported.

https://doi.org/10.1016/j.ajpath.2021.10.017

acid metabolism.[11] These findings indicate that ZFP36L1 may play critical roles in regulating liver metabolic homeostasis. However, the detailed physiological functions of ZFP36L1 remain particularly elusive, partly due to the embryonic lethal phenotype that is observed following germline deletion of ZFP36L1 in mice.[4]

This study sought to understand the physiological roles of ZFP36L1 in the liver. It was hypothesized that the removal of ZFP36L1 could alter certain pathological processes associated with liver. To test this, Cre-Lox technology was employed to delete *Zfp36l1* in hepatocytes and cholangiocytes.[12] Liver-specific ZFP36L1-deficient ($L1^{LKO}$) mice and their littermate control mice ($L1^{FLX}$) were then subjected to a model of alcoholic steatohepatitis.[13] The mice were analyzed for histologic, biochemical, and transcriptional alterations associated with the development of alcoholic steatosis, liver injury, and inflammation. The results show a novel protective effect of liver-specific ablation of ZFP36L1 against alcohol-induced steatosis and liver inflammation, and identified *Fgf21* mRNA as a likely target of ZFP36L1.

Materials and Methods

Mice

The floxed mice carrying loxP-flanked exon 2 of *Zfp36l1* alleles were generated by gene targeting in C57BL/6 embryonic stem cells at Xenogen Biosciences (Cranbury, NJ). Liver-specific *Zfp36l1* knockout ($Zfp36l1^{flox/flox}$/Cre^{+}; $L1^{LKO}$) mice were generated by crossing the homozygous floxed mice ($Zfp36l^{flox/flox}$) with albumin-Cre (Alb-Cre)[14] mice (Jackson Laboratory, Bar Harbor, ME). Genotype status of the progeny was determined by PCR using primer 1 (P1), 5′-CTCTTGCTGGTCACTACCGTCGCT-3′ and primer 2 (P2), 5′-TCAATGTAAGCCAGCAAGTGCAGC-3′, which amplified a 484-bp endogenous *Zfp36l1* wild-type (WT) allele and a 618-bp mutant *Zfp36l1* floxed allele. PCR conditions were 93°C for 3 minutes followed by 30 cycles of 93°C for 30 seconds, 58°C for 30 seconds, and 72°C for 1 minute, with a final extension of 72°C for 10 minutes. Eight- to 12-week−old female $L1^{LKO}$ and littermate control ($Zfp36l1^{flox/flox}$/Cre^{-}; $L1^{FLX}$) mice were used in all studies. All the animal experiments were performed in accordance with principles and procedures outlined in the NIH *Guide for the Care and Use of Laboratory Animals*[15] and were approved by the Louisiana State University Animal Care and Use Committee.

Lieber-DeCarli Liquid Diet Model of Chronic-Plus-Binge Model of Alcoholic Liver Disease

Eight- to 12-week−old female $L1^{LKO}$ or $L1^{FLX}$ mice were subjected to alcoholic liver disease as described by Bertola et al.[13] Briefly, mice were first acclimatized for 5 days to tube feeding and liquid diet *ad libitum*. Following acclimatization, mice were maintained for 10 days on a fresh liquid diet (free access) containing 5% ethanol (v/v) (Lieber-DeCarli ‘82 Shake and Pour ethanol liquid diet; product number F1258SP; Bio-Serv, Flemington, NJ) or pair-fed with a control isocaloric diet (Lieber-DeCarli ’82, Shake and Pour control liquid diet; product number F1259SP; Bio-Serv) in which the same number of calories was obtained from dextrin maltose. The freshly constituted liquid diet was stored in the refrigerator and used within 3 days. The refrigerated diet was brought to room temperature, and a calculated volume of fresh ethanol was added daily. On day 11, a single intragastric (oral gavage) administration of ethanol (5-g ethanol/kg body weight; 31.5% ethanol) or an isocaloric dose of maltose-dextrin (control group) was administered between 8 AM and 9 AM. Mice were humanely euthanized 9 hours after gavage feeding, and serum and liver were collected.

Necropsy and Tissue Collection

Mice were humanely euthanized, midline laparotomy was performed, and blood was then collected by cardiac puncture for serum. The livers were removed and weighed, and the left lateral lobe was dissected into three parts, of which the first part was stored in RNAlater (Life Technologies, Carlsbad, CA), the second part was snap-frozen and stored at −80°C, and the third part was fixed in 10% neutral buffered formalin. The remaining liver lobes were fixed in 10% neutral buffered formalin.

Histology

The 5-μm sections of liver were stained with hematoxylin and eosin for routine histologic analyses. Quantification of steatosis was performed by stereological point counting.[16] Briefly, the histologic microscopic images were overlaid by a regular grid of points. The grid contained approximately 300 intersections within the tissue boundary that were counted as either fat deposits or no fat deposits depending on whether they covered the fat droplets or not. The fractional area of fat droplets was determined by dividing the number of points covering fat droplets to the total number of points.

Oil Red O Staining

Oil Red O staining was used to confirm hepatic steatosis. Briefly, freshly collected liver tissue was embedded in optimal cutting temperature compound (Sakura Finetek, Torrance, CA), frozen on dry ice, and then stored at −80°C. Later, 10 μm sections were obtained with a cryostat and fixed with 10% neutral buffered formalin, washed thoroughly with running tap water for 5 minutes, and then stained in Oil Red O solution (Electron Microscopy Sciences, Hatfield, PA) for 8 minutes followed by rinsing in 60% isopropanol and counterstaining with Harris

hematoxylin for 1 minute. Sections were then mounted with glycerol jelly medium.

Immunohistochemistry

Immunohistochemical stainings for myeloperoxidase (MPO) and F4/80 were performed on formalin-fixed, paraffin-embedded liver sections. Briefly, liver sections were first deparaffinized with Citrisolv (Decon Labs Inc., King of Prussia, PA) (2×5 minutes each) and were rehydrated through descending grades of ethanol (100%, 95%, 70%, 30%, distilled water; 3 minutes each). Antigen retrieval was performed using a proteinase K–mediated antigen retrieval method. Endogenous peroxides were quenched with 3% hydrogen peroxide solution for 10 minutes at room temperature. Sections were blocked for 20 minutes with bocking serum followed by incubation in the primary antibodies [rabbit anti-mouse myeloperoxidase monoclonal antibody (ab208670; Abcam, Waltham, MA) and rat anti-mouse F4/80 antibody (MCA497G; Bio-Rad, Hercules, CA)] at room temperature for 1 hour. Sections were washed and incubated with respective biotinylated secondary antibodies for 1 hour at room temperature. The sections were then rinsed in deionized water (2×5 minutes each) and processed using VECTASTAIN Elite ABC HRP Kits (PK-6101/6104; Vector Laboratories, Burlingame, CA), followed by chromogenic substrate conversion using ImmPACT NovaRED HRP Substrate Kit (SK-4800; Vector Laboratories). Sections were counterstained with Gill's Hematoxylin-I (EMD Millipore Corporation, Burlington, MA) for 30 seconds, rinsed in deionized water, dehydrated with ascending grades of ethanol, and coverslipped with VectaMount mounting media (H-5000; Vector Laboratories).

Liver Triglyceride Assay

Liver triglyceride levels were measured using Triglyceride Assay Kit (ab65336; Abcam) per the manufacturer's recommendations. Briefly, 30 mg liver tissue samples were heated in 400 μL of 5% NP-40 solution (VWR chemicals, Solon, OH) at 90°C for 5 minutes to dissolve triglycerides. The heating cycles were repeated until a clear lysate was obtained by centrifugation. The triglyceride levels were then determined in liver lysates in duplicates and quantified at 570 nm using Spark Multimode Microplate Reader (Tecan Trading AG, Mannedorf, Switzerland). Liver triglyceride values were calculated and expressed as mg/g of the liver tissue.

Serum Enzymes and Lipids Analyses

Analyses for alanine transaminase (ALT), aspartate transaminase (AST), cholesterol, and triglycerides were performed on a Beckman Coulter AU680 chemistry analyzer using Beckman Coulter reagents (Beckman-Coulter, Irving, TX) at the clinical pathology core at Louisiana State University.

Enzyme-Linked Immunosorbent Assay

Serum levels of fibroblast growth factor (FGF21) were determined using an enzyme-linked immunosorbent assay kit (R&D systems, Minneapolis, MN) according to the manufacturer's instructions. The optical density was measured at 450 nm and 570 nm using Spark Multimode Microplate Reader (Tecan Trading AG, Mannedorf, Switzerland). The optical density readings at 570 nm were subtracted from those at 450 nm to correct for optical imperfections in the plate.

RNA Extraction

Total RNA was extracted using the GE Healthcare Illustra RNAspin MiniRNA isolation kit, according to the manufacturer's instructions (GE Healthcare, Little Chalfont, UK). The RNA content and purity were determined by measuring absorbance at 260 nm and 260/280 ratio, respectively, on a NanoDrop 8000 spectrophotometer (Thermo Fisher Scientific, Waltham, MA). The quality of the RNA was determined using an Agilent 2100 Bioanalyzer (Agilent, Santa Clara, CA).

Quantitative PCR

RT-qPCR for the quantification of *Tnf, Mcp1, Il10,* and *Cd36* transcripts was performed using the SYBR Green method. Briefly, 1 μg of total RNA was used for cDNA synthesis using an iScript cDNA synthesis kit (Bio-Rad). Quantitative real-time RT-PCR was performed on the ABI Prism 7900 Sequence Detection System (Applied Biosystems, Waltham, MA). Primer sequences were: *Tnf,* forward 5′-CTTCTGTCTACTGAACTTCGGG-3′, reverse 5′-CAGGCTTGTCACTCGAATTTTG-3; *Mcp1*, forward 5′-GTCCCTGTCATGCTTCTGG-3′, reverse 5′-GC TCTCCAGCCTACTCATTG-3′; *Il10*, forward 5′-AGCCGG GAAGACAATAACTG-3′, reverse 5′-GGAGTCGGTTAG-CAGTATGTTG-3′; *Cd36*, forward 5′-GCGACATGAT TAATGGCACAG-3′, reverse 5′-GATCCGAACACAGC GTAGATAG-3′.

The C_T values were normalized to *Gapdh* internal controls. The expression levels were calculated according to the $2^{-\Delta\Delta C_T}$ method. Quantitative PCR for *Fgf21* and *Zfp36l1* was performed using Taqman assays (*Fgf21*:hs00173927; *Zfp36l1*: hs00245183).

Library Preparation and RNA Deep Sequencing

Library preparation and RNA sequencing was performed at Novogene Corporation Inc. (Sacramento, CA). Briefly, 1 μg of RNA was used for cDNA library construction using an NEBNext Ultra II RNA Library Prep Kit for Illumina (New England Biolabs, Ipswich, MA) according to the manufacturer's protocol. mRNA was enriched using oligo (dT) beads followed by two rounds of purification and random

fragmentation. The first-strand cDNA was synthesized using random hexamers followed by generation of the second strand. After a series of terminal repair, polyadenylation, and sequencing adaptor ligation, the double-stranded cDNA library was completed following size selection and PCR enrichment. The resulting 250- to 350-bp insert libraries were quantified using a Qubit 2.0 fluorometer (Thermo Fisher Scientific) and quantitative PCR. Size distribution was analyzed using an Agilent 2100 Bioanalyzer (Agilent Technologies). Qualified libraries were sequenced on an Illumina NovaSeq 6000 Platform (Illumina, Inc., San Diego, CA) using a paired-end 150 run (2 × 150 bases). Approximately 20 M raw reads were generated from each library.

Immunoblotting

Cells/tissues were lysed using Pierce RIPA buffer (Thermo Fisher Scientific) supplemented with Pierce protease inhibitor mixture (Thermo Fisher Scientific) and phosphatase inhibitors (10 mM sodium fluoride and 1 mM sodium orthovanadate). Tissues were mechanically homogenized using a homogenizer (Fisherbrand 150 handheld homogenizer; Thermo Fisher Scientific). Tissue lysates were centrifuged (13,000 × *g*, 10 minutes, 4°C) to remove insoluble material, and protein concentrations of the supernatants were measured using the Bradford assay (Bio-Rad Laboratories). Denatured proteins were separated on a 4% to 12% Bis-Tris plus gel (Invitrogen, Carlsbad, CA), transferred onto polyvinylidene difluoride membranes (Invitrogen), and probed with a 1:1000 dilution of BRF1/2 primary antibody (Cell Signaling Technology, Danvers, MA), followed by a 1:3000 dilution of horseradish peroxidase–conjugated goat anti-rabbit IgG. Signals were determined either on a ChemiDoc Imaging System (Bio-Rad Laboratories) or on X-ray film.

Luciferase Reporter Assay

HEK293 cells were procured from ATCC (Manassas, VA). Cells were cultured in EMEM with 10% FBS. pcDNA 3.1+/C-(K)-DYK *Zfp36l1*, pcDNA 3.1+/C-(K)-DYK *Zfp36l1*-zinc finger mutant C135R, C173R (two amino-acid mutations within the two zinc fingers at positions 135 and 173), and pcDNA 3.1+/C-(K)-DYK empty vector were obtained from GenScript Biotech (Piscataway, NJ). Ambion pMIR-REPORT Luciferase expression reporter vector was obtained from Thermo Fisher Scientific, and the 3′UTR of *Ffg21* mRNA was cloned into a pMIR-REPORT luciferase reporter vector. Transfections were done with Lipofectamine reagent (Invitrogen). Luminescence was determined using a Promega Luciferase Reporter Assay Kit (Promega, Madison, WI), according to the manufacturer's instructions, on a Spark multimode microplate reader (Tecan Trading AG, Mannedorf, Switzerland). Briefly, cells were seeded onto 6-well plates and transfected with the respective constructs (0.5 μg) when they reached a confluency of approximately 60% to 65%. At 48 hours after transfection, the growth medium was removed, and cells were gently rinsed with phosphate-buffered saline, followed by addition of 1× reporter lysis buffer to lyse the cells. To ensure complete lysis, cells were subjected to a single freeze–thaw cycle. Lysed cells were scraped, transferred into microcentrifuge tubes, and then centrifuged at 12,000 × *g* for 15 seconds at room temperature. The supernatants were transferred into new microcentrifuge tubes. A total of 20 μL of cell lysate was used per well of a 96-well plate for luciferase assays. The Spark multimode microplate reader was programed to add 100 μL of luciferase assay reagent per well with the injector. Luminescence was determined immediately (10 seconds). Luminescence was normalized to beta-galactosidase measurements.

Cotransfection Assay

For cotransfection assays, HEK293 cells were cotransfected with pcDNA 3.1+/C-(K)-DYK empty vector alone, the pcDNA 3.1+/C-(K)-DYK *Zfp36l1*-WT plasmid or the zinc finger mutant, pcDNA 3.1+/C-(K)-DYK *Zfp36l1*-C135R, C173R, and the full-length pcDNA 3.1+/C-(K)-DYK-*Fgf21*plasmid, which contained an intact 3′UTR (GenScript Biotech). Two concentrations of *Zfp36l1* (WT and mutant) plasmids were used, 0.25 μg and 0.50 μg, whereas 0.5 μg of the *Fgf21* plasmid was transfected in all. The amount of total transfected plasmid was kept constant for all the plates, and normalized by the addition of vector control plasmid. The cells were harvested after 48 hours, RNA was isolated, cDNA was prepared using iScript Reverse Transcription Supermix (Bio-Rad Laboratories), and then the levels of *Fgf21* and *Zfp36l1* mRNAs were assessed by quantitative real-time PCR.

Electrophoretic Mobility Shift Assays

RNA-ARE probes were designed from the *Fgf21*-3′UTR ARE sequence and synthesized with 5′-biotin–end labelling (Integrated DNA Technologies, Coralville, IA). HEK293 cells were transfected with the ZFP36L1 expression plasmid (pcDNA 3.1+/C-(K)-DYK *Zfp36l1*) or its zinc finger mutant (pcDNA 3.1+/C-(K)-DYK *Zfp36l1*-C135R, C173R), and cytosolic cell extracts were prepared. Briefly, the transfection mixture was removed, and cells were rinsed with ice-cold Ca^{2+}- and Mg^{2+}-free Dulbecco's phosphate-buffered saline. The cells were then scraped and centrifuged at 600 × *g* for 3 minutes at 4°C. The supernatants were removed, and the pellets were rinsed with ice-cold diethyl-pyrocarbonate–treated water containing 8 μg/mL leupeptin, 0.2 mM phenylmethylsulfonyl fluoride, and 1 μg/mL pepstatin A. The cells were then lysed in a hypotonic cell lysis buffer containing 10 mM HEPES (pH 7.6), 5 mM KCl, 5% (v/v) glycerol, 0.25% (v/v) Nonidet P-40, 1 μg/mL

pepstatin A, 0.1 mM phenylmethylsulfonyl fluoride, and 8 μg/mL leupeptin. Lysates were centrifuged for 15 minutes at 15,000 × *g* at 4°C. The supernatant was transferred to a fresh tube, and potassium chloride and glycerol were added to final concentrations of 40 mM and 15% (v/v), respectively. Cell extracts were aliquoted and stored at −80°C until ready to use. For the electrophoretic mobility shift assay, approximately 8 μg of cytosolic extracts prepared from HEK293 cells transfected with either the vector alone, or with the WT or mutant ZFP36L1 expression constructs, were incubated with 300 mM 5′-biotin−end-labelled ARE probes at room temperature for 30 minutes. The total reaction volume was 20 μL and consisted of 10 mM HEPES (pH 7.6), 40 mM KCl, 2.5% (v/v) glycerol, 3 mM $MgCl_2$, 2.5 μg/μL heparin, and 50 ng/μL yeast tRNA. Following incubation, the reaction mixture was loaded onto 6% to 8% nondenaturing acrylamide gels and subjected to electrophoresis (120 V for 60 minutes in 0.5× Tris/borate/EDTA buffer). Gels were transferred onto Biodyne B nylon membranes (0.45 μm; Thermo Fisher Scientific) in 0.5× Tris/borate/EDTA buffer (60 V for 30 minutes). RNA−protein complexes and the unbound RNA probe were detected using the Chemiluminescent Nucleic Acid Detection Module (Thermo Fisher Scientific), following the manufacturer's instructions.

Statistical Analysis

Statistical significance between two groups was determined by *t*-test assuming unequal variance. Significant differences among groups were determined by one-way analysis of variance followed by Tukey's post hoc test for multiple comparisons. All data are expressed as means ± SEM. $P < 0.05$ is considered statistically significant. Statistical analyses were performed using GraphPad Prism software version 7.0 (GraphPad Software, La Jolla, CA).

Nucleotide Sequence Accession Number

The RNA-Seq data have been deposited in the NCBI Gene Expression Omnibus database (*https://www.ncbi.nlm.nih.gov/geo*; accession number GSE163444).

Results

Generation and Characterization of ZFP36L1 Liver-Specific Knockout Mice

To investigate the role of ZFP36L1 in liver, liver-specific *Zfp36l1*-deficient mice ($L1^{LKO}$) were generated using the Cre-LoxP recombination approach. RNA-Seq analysis of liver RNA showed at least a fivefold reduction in the mRNA levels of *Zfp36l1* in $L1^{LKO}$ mice compared with littermate control $L1^{FLX}$ mice (Figure 1A). Western blot analysis of liver tissue lysates showed minimal to no detectable expression of ZFP36L1 in $L1^{LKO}$ mice compared with littermate control $L1^{FLX}$ mice (Figure 1B). Quantitatively, the expression of ZFP36L1 was significantly reduced in $L1^{LKO}$ mice compared with littermate control $L1^{FLX}$ mice (Figure 1C). The $L1^{LKO}$ mice developed normally and did not exhibit any growth defects or anatomic or histologic abnormalities (data not shown).

Alcohol Diet−Fed $L1^{LKO}$ Mice Exhibit Significantly Attenuated Hepatic Steatosis, Injury, and Inflammation Compared with Alcohol Diet−Fed Littermate Control $L1^{FLX}$ Mice

In order to determine the effect of ZFP36L1 deletion in stressed liver cells, $L1^{FLX}$ and $L1^{LKO}$ mice were subjected to alcohol-induced liver injury and steatosis by feeding them the alcohol-containing Lieber-DeCarli diet (alcohol group). The weights of both the $L1^{FLX}$ and $L1^{LKO}$ mice did not change significantly after alcohol ingestion over a period of

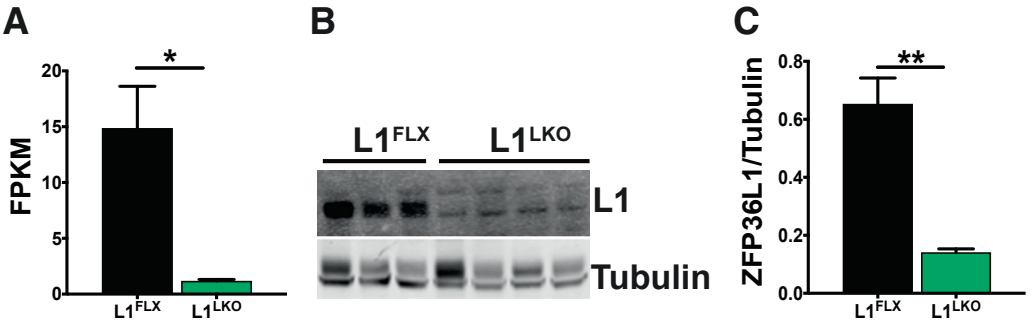

Figure 1 mRNA and protein expression of ZFP36L1 in control ($L1^{FLX}$) versus ZFP36L1 liver-specific knockout ($L1^{LKO}$) mice. **A:** FPKM (fragments per kilobase of transcripts per million mapped reads) values from liver RNA-Seq data showing the expression of *Zfp36l1* mRNA in liver homogenates from ZFP36L1-sufficient ($L1^{FLX}$) and liver-specific ZFP36L1-deficient ($L1^{LKO}$) mice. **B:** An immunoblot showing expression of ZFP36L1 in liver homogenates from ZFP36L1-sufficient ($L1^{FLX}$) and liver-specific ZFP36L1-deficient ($L1^{LKO}$) mice. **C:** Quantification of immunoblots shown in **panel B** was performed using ImageJ version 1.53i (NIH, Bethesda, MD; *https://imagej.nih.gov/ij*). Data are expressed as means ± SEM. $n = 4$ mice (**A**); $n = 3$ $L1^{FLX}$ mice (**B**); $n = 4$ $L1^{LKO}$ mice (**B**). $^*P < 0.05$, $^{**}P < 0.01$ (unpaired *t*-test).

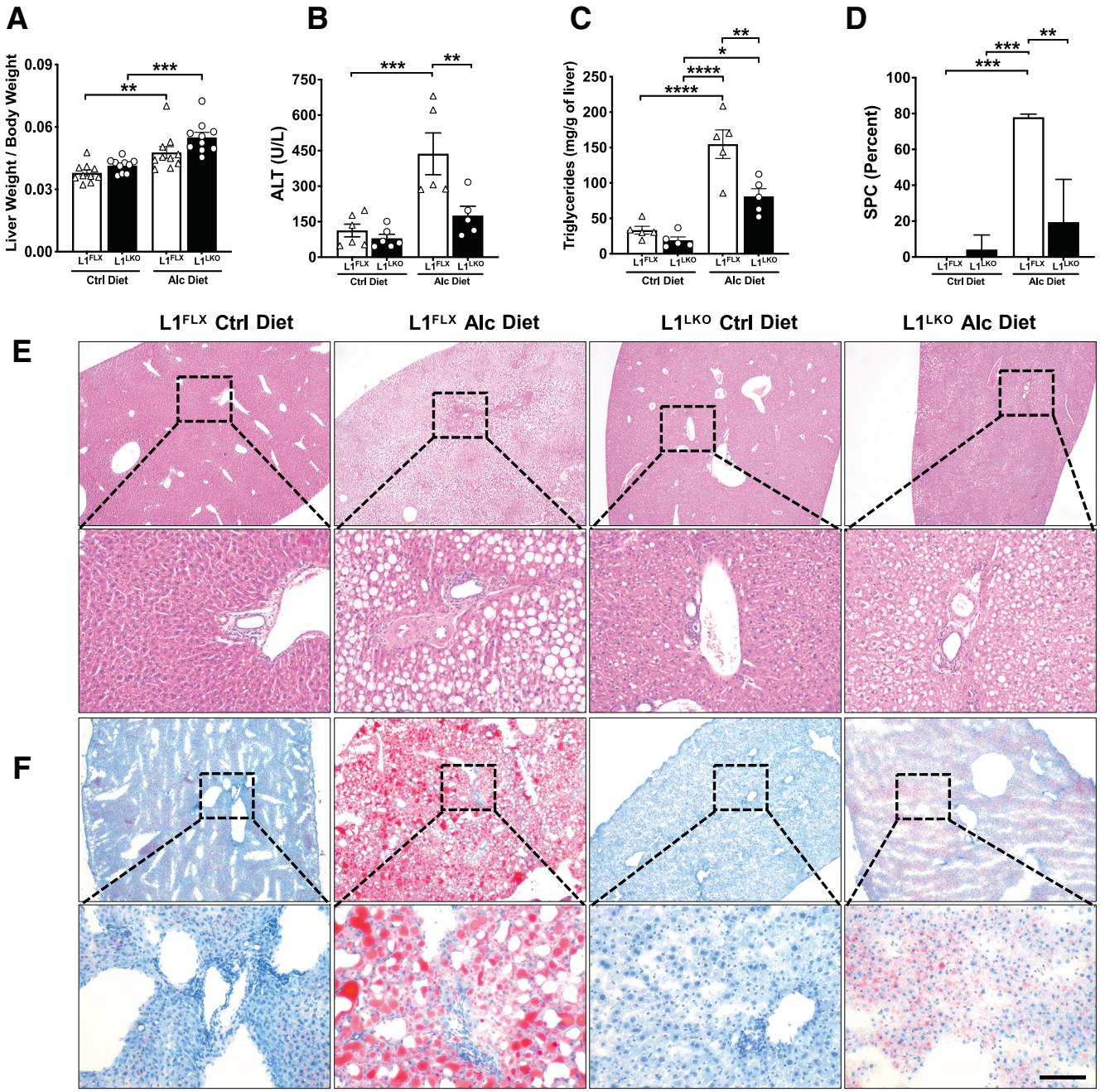

Figure 2 ZFP36L1 LKO mice are protected from alcohol-induced liver injury. **A:** Liver weight to body weight ratios of alcohol diet—fed ZFP36L1-sufficient ($L1^{FLX}$) and liver-specific ZFP36L1-deficient ($L1^{LKO}$) mice and those that were pair-fed with control diet. **B:** Serum levels of alanine transaminase (ALT) in alcohol diet—fed ZFP36L1-sufficient ($L1^{FLX}$) and liver-specific ZFP36L1-deficient ($L1^{LKO}$) mice and the control diet—fed ZFP36L1-sufficient ($L1^{FLX}$) and liver-specific ZFP36L1-deficient ($L1^{LKO}$). **C:** Liver triglyceride levels in alcohol diet—fed ZFP36L1-sufficient ($L1^{FLX}$) and liver-specific ZFP36L1-deficient ($L1^{LKO}$) mice and the control diet—fed ZFP36L1-sufficient ($L1^{FLX}$) and liver-specific ZFP36L1-deficient ($L1^{LKO}$) mice. **D:** Quantification of hepatic steatosis of images shown in **E**. **E:** Representative liver histology images from ZFP36L1-sufficient ($L1^{FLX}$) and liver-specific ZFP36L1-deficient ($L1^{LKO}$) mice that were fed with alcohol diet versus those that were pair-fed with control diet are shown. **F:** Oil Red O—stained liver sections from ZFP36L1-sufficient ($L1^{FLX}$) and liver-specific ZFP36L1-deficient ($L1^{LKO}$) mice that were fed with alcohol diet versus those that were pair-fed with control diet are shown. Representative images from three independent experiments are shown. **Boxed areas** in **E** and **F** are shown at higher magnification below. Data are expressed as means ± SEM. $n = 10$ mice in each group (**A**); $n = 5$ mice in the alcohol-diet group (**B**); $n = 6$ mice in the control diet group (**B**); $n = 5$ mice (**C**); $n = 3$–4 (**D**). $^{*}P < 0.05$, $^{**}P < 0.01$, $^{***}P < 0.001$, and $^{****}P < 0.0001$ (one-way analysis of variance followed by Tukey's correction for multiple comparisons). Scale bar = 50 μm. Alc, alcohol; Ctrl, control.

11 days compared with their initial body weights (Supplemental Figure S1A). Alcohol significantly increased the liver weight to body weight ratio after alcohol-diet feeding in both $L1^{FLX}$ and $L1^{LKO}$ mice, but the difference was not significant between the alcohol diet—fed $L1^{FLX}$ and $L1^{LKO}$ groups (Figure 2A).

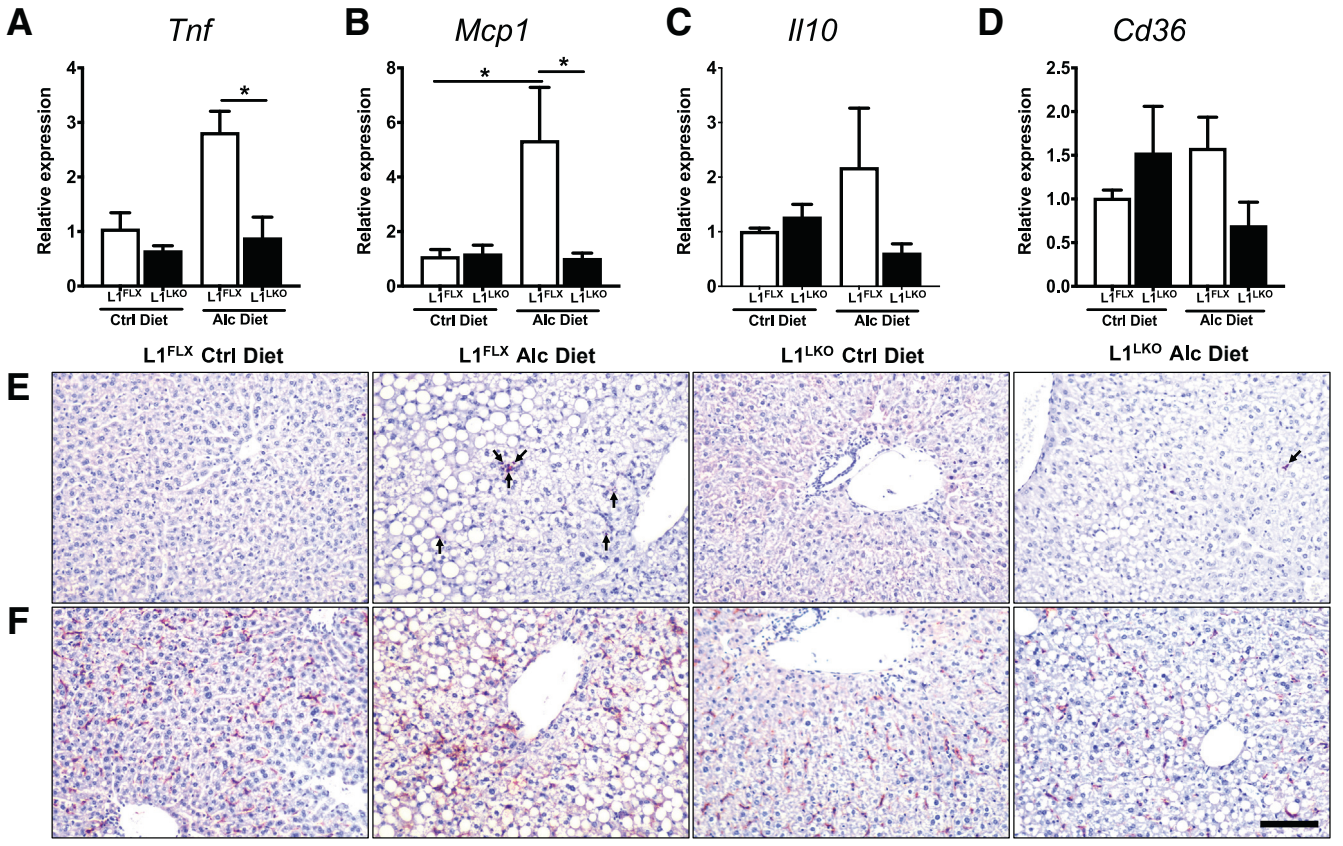

Figure 3 ZFP36L1 LKO mice were protected from alcohol-induced liver inflammation. Relative quantification of *Tnf* (**A**), *Mcp1* (**B**), *Il10* (**C**), and *Cd36* (**D**) mRNA expression in the liver homogenates from alcohol diet–fed ZFP36L1-sufficient ($L1^{FLX}$) and liver-specific ZFP36L1-deficient ($L1^{LKO}$) mice, and those that were pair-fed with control diet. Representative photomicrographs of myeloperoxidase (MPO) (**E**) and F4/80 (**F**) stained liver sections from alcohol diet–fed ZFP36L1-sufficient ($L1^{FLX}$) and liver-specific ZFP36L1-deficient ($L1^{LKO}$) mice and those that were pair-fed with control diet. **Arrows** depict cells that stained positive for MPO. Data are expressed as means ± SEM. $n = 3$ to 4 mice. $^*P < 0.05$ (one-way analysis of variance followed by Tukey's correction for multiple comparisons). Scale bar = 50 μm. Alc, alcohol; *Cd36*, cluster of differentiation 36; Ctrl, control; *Il10*, interleukin-10; *Mcp1*, monocyte chemoattractant protein-1; *Tnf*, tumor necrosis factor.

Alcohol results in hepatic lesions, particularly steatosis, hepatic injury, and hepatic inflammation.[17] Serum levels of ALT, a marker of liver injury, were significantly increased in alcohol diet–fed $L1^{FLX}$ mice compared with control diet–fed (pair-fed) $L1^{FLX}$ mice. However, alcohol ingestion did not increase the levels of ALT in $L1^{LKO}$ mice (Figure 2B). The levels of AST were also increased in alcohol diet–fed mice, but the difference was not statistically significant between the $L1^{FLX}$ and $L1^{LKO}$ groups (Supplemental Figure S1B). Liver triglycerides were significantly increased in alcohol diet–fed $L1^{FLX}$ and $L1^{LKO}$ mice compared with their respective control diet–fed (pair-fed) counterparts. However, the levels of liver triglycerides were significantly less in alcohol diet–fed $L1^{LKO}$ compared with alcohol diet–fed $L1^{FLX}$ mice (Figure 2C). The serum levels of triglycerides and cholesterol were not significantly increased after alcohol diet feeding compared with control diet feeding in either of the two genotype groups (Supplemental Figure S1, C and D).

Steatosis is the earliest response of the liver to alcohol ingestion and is characterized by the accumulation of lipid droplets within the hepatocytes, starting at the centrilobular areas and progressing toward the mid-lobular and periportal regions in later stages.[17,18] Consistent with these reports, the alcohol diet significantly increased microvesicular and macrovesicular steatosis in $L1^{FLX}$ mice compared with control diet–fed $L1^{FLX}$ mice. Remarkably, alcohol diet–fed $L1^{LKO}$ mice exhibited markedly diminished hepatic steatosis compared with the alcohol diet–fed $L1^{FLX}$ mice (Figure 2, D–F).

Alcohol-induced steatosis is usually accompanied by hepatic inflammation.[17] Certain proinflammatory mediators, particularly tumor necrosis factor (TNF) and MCP1, have been implicated in alcoholic liver inflammation.[19,20] Similarly, IL-10 and CD36, a fatty acid translocase, have also been shown to play a role in alcoholic liver disease.[21,22] Therefore, mRNA expression levels for these proinflammatory cytokines and mediators were assessed in alcohol diet–fed $L1^{FLX}$ and $L1^{LKO}$ mice. The mRNA expression levels of both *Tnf* and *Mcp1* were significantly increased in alcohol diet–fed $L1^{FLX}$ mice compared with control diet–fed $L1^{FLX}$ mice (Figure 3, A and B). However, the increase in expression of *Tnf* and *Mcp1* was significantly attenuated in alcohol diet–fed $L1^{LKO}$ mice compared with

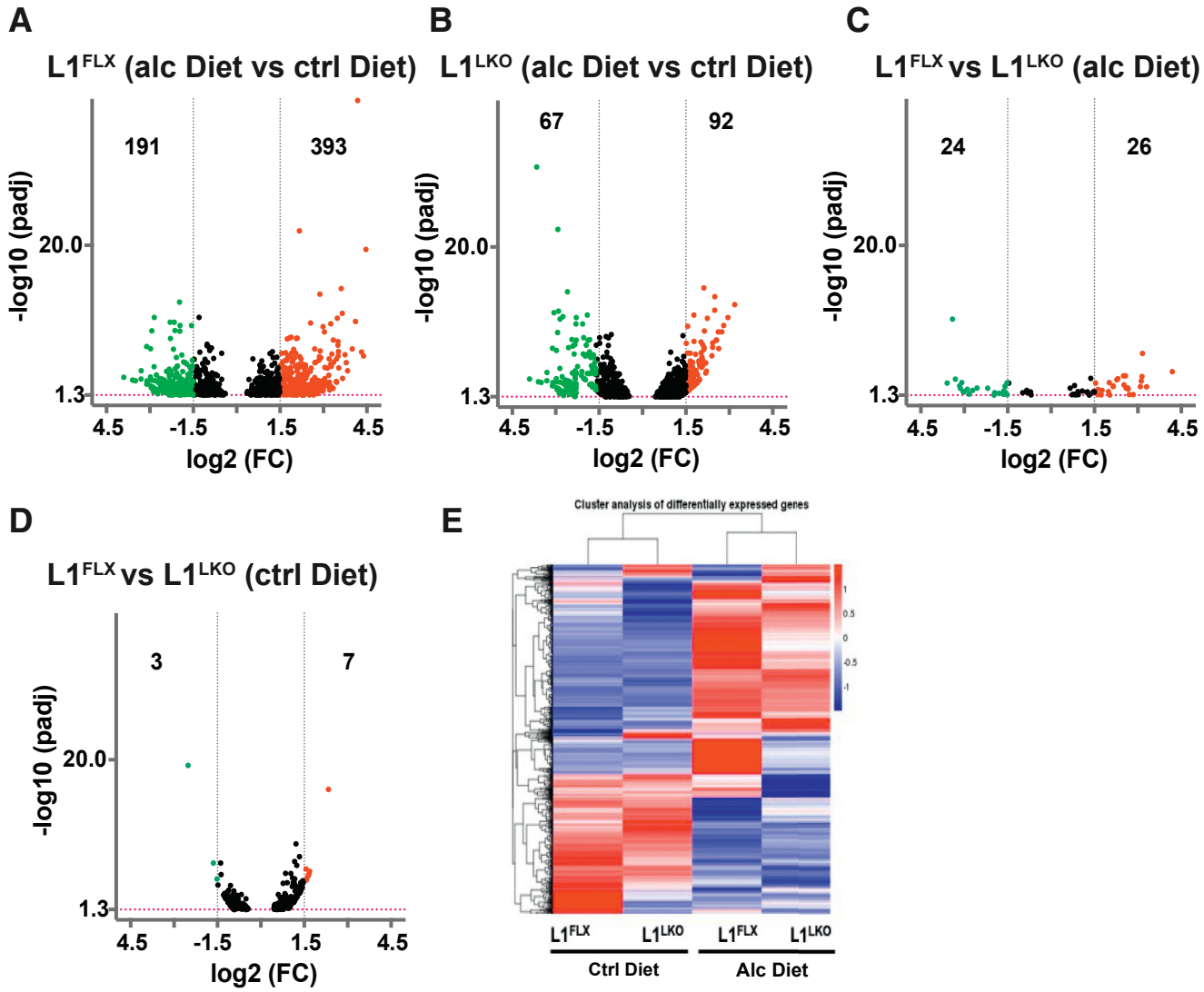

Figure 4 Differentially expressed transcripts in $L1^{LKO}$ mice and $L1^{FLX}$ mice following control diet and alcohol diet feeding. Volcano plots depict differentially expressed transcripts (red: up-regulated; green: down-regulated) in alcohol diet–fed versus control diet–fed $L1^{FLX}$ mice (**A**); alcohol diet–fed versus control diet–fed $L1^{LKO}$ mice (**B**); alcohol diet–fed $L1^{FLX}$ versus $L1^{LKO}$ mice (**C**); and control diet–fed $L1^{FLX}$ versus $L1^{LKO}$ mice (**D**). **Black vertical dashed lines** indicate a log2fold-change cutoff of 1.5. The **red horizontal dashed line** indicates −log10 (*P* value) cutoff of 1.3 ($P = 0.05$). Heat map of differentially expressed transcripts from alcohol diet–fed ZFP36L1-sufficient ($L1^{FLX}$) and liver-specific ZFP36L1-deficient ($L1^{LKO}$) mice, and control diet–fed ZFP36L1-sufficient ($L1^{FLX}$) and liver-specific ZFP36L1-deficient ($L1^{LKO}$) mice (**E**). Alc, alcohol; Ctrl, control; FC, fold change.

alcohol diet–fed $L1^{FLX}$ mice (Figure 3, A and B). The mRNA expression levels of *Il10* and *Cd36* also showed similar trends, but the differences were not statistically significant between alcohol diet–fed $L1^{LKO}$ and alcohol diet–fed $L1^{FLX}$ mice (Figure 3, C and D). Increased inflammation in alcohol diet–fed $L1^{FLX}$ mice was also evident from increased staining for neutrophils [MPO-positive] in this group compared with control diet–fed $L1^{FLX}$ mice. The alcohol diet–fed $L1^{LKO}$ mice had fewer numbers of neutrophils in tissue sections compared with alcohol diet–fed $L1^{FLX}$ mice (Figure 3E). There were no differences in the numbers of F4/80-positive macrophages within the liver tissue sections (Figure 3F). Taken together, these data demonstrate that liver-specific deletion of ZFP36L1 confers significant protection against hepatic steatosis, hepatic injury, and hepatic inflammation in alcohol diet–fed mice.

ZFP36L1 Deficiency Results in Reduced Numbers of Differentially Expressed Transcripts in Alcohol Diet–Fed Mice

In order to identify transcriptomic changes through which ZFP36L1 modulates alcoholic hepatic steatosis, hepatic injury, and hepatic inflammation, RNA-Seq analysis of total liver RNA obtained from the four groups: control diet–fed and alcohol diet–fed $L1^{FLX}$ and $L1^{LKO}$ mice was performed. The RNA-Seq data are expressed as fragments per kilobase per million mapped reads. The inclusion criteria for increase or decrease were set as greater than or less than 1.5-

Table 1 Inflammatory Genes

Gene symbol	Gene name	$L1^{FLX}$ alcohol diet vs ctrl diet (log2FC)	$L1^{FLX}$ alcohol diet vs ctrl diet (padj)	$L1^{LKO}$ alcohol diet vs ctrl diet (log2FC)	$L1^{LKO}$ alcohol diet vs ctrl diet (padj)
TLR4 receptor					
Cd14	CD14 antigen	**3.0**	**6.53^{-10}**	1.1	NA
Macrophage receptor					
Marco	Macrophage receptor with collagenous structure	**1.6**	**1.81^{-05}**	0.1	0.89227
Interleukin receptor					
Il3ra	Interleukin 3 receptor alpha chain	**2.4**	**0.01761**	-0.5	0.24085
Chemokines					
Ccl2	Chemokine (C-C_motif) ligand 2	**3.0**	**1.76^{-05}**	0.6	NA
Ccr1	Chemokine (C-C_motif) receptor 1	**2.9**	**0.00231**	0.6	0.38265
Cxcl2	Chemokine (C-X-C_motif) ligand 2	**1.9**	**0.04027**	0.5	NA
Cxcl14	Chemokine (C-X-C_motif) ligand 14	**1.5**	**0.01405**	0.6	0.33444
Ccrl2	Chemokine (C-C_motif) receptor-like 2	**1.5**	**0.00243**	0.4	0.55244
Ccl9	Chemokine (C-C_motif) ligand 9	**1.4**	**0.00053**	**0.8**	**0.05965**
TNF superfamily					
Tnfrsf12a	Tumor necrosis factor receptor superfamily member 12a	**2.5**	**2.12^{-05}**	**1.8**	**0.00100**
Tnfrsf10b	Tumor necrosis factor receptor superfamily member 10b	**2.3**	**0.03836**	0.8	0.25032
Tnfrsf23	Tumor necrosis factor receptor superfamily member 23	**2.1**	**0.00451**	**1.2**	**0.03907**
Tnfrsf21	Tumor necrosis factor receptor superfamily member 21	**0.8**	**0.00636**	0.2	0.76364
Tnfaip1	Tumor necrosis factor alpha-induced protein 1 (endothelial)	**0.8**	**8.79^{-06}**	**0.6**	**0.08765**
NFkB family					
Relb	Avian reticuloendotheliosis viral (v-rel) oncogene related B	**1.4**	**0.00535**	**1.1**	**0.05787**
Rell1	RELT-like 1	**1.2**	**0.02623**	**1.1**	**0.00801**
Ikbip	IKBKB interacting protein	**1.0**	**0.00159**	0.7	0.18132
Nfkbib	Nuclear factor of kappa light polypeptide gene enhancer in B cells inhibitor beta	**0.6**	**0.04846**	0.4	0.36545
MAP kinase family					
Mapk4	Mitogen activated protein kinase 4	**2.2**	**0.01868**	0.9	0.15484
Map3k6	Mitogen activated protein kinase kinase kinase 6	**1.9**	**0.04403**	**0.9**	**0.09448**
Complement components					
C5ar1	Complement component 5a receptor 1	**2.7**	**4.26^{-06}**	**1.5**	**0.00133**

(*table continues*)

Table 1 (*continued*)

Gene symbol	Gene name	$L1^{FLX}$ alcohol diet vs ctrl diet (log2FC)	$L1^{FLX}$ alcohol diet vs ctrl diet (padj)	$L1^{LKO}$ alcohol diet vs ctrl diet (log2FC)	$L1^{LKO}$ alcohol diet vs ctrl diet (padj)
C3ar1	Complement component 3a receptor 1	**1.5**	**0.00041**	0.7	0.24271
Cell-surface proteins					
Cd63	CD63 antigen	**2.9**	**1.10^{-06}**	**1.4**	**0.00210**
Cd34	CD34 antigen	**1.3**	**0.03684**	0.5	0.45291
Cd68	CD68 antigen	**1.1**	**0.01152**	-0.1	0.86209
Cd44	CD44 antigen	**0.9**	**0.03224**	0.2	0.67557
Protein kinase substrate protein					
Marcksl1	MARCKS-like_1	**0.7**	**0.00503**	0.3	0.47187
Metalloelastases					
Mmp12	Matrix metallopeptidase_12	**3.4**	**2.95^{-08}**	1.1	NA
Timp1	Tissue inhibitor of metalloproteinase 1	**2.9**	**0.00165**	0.6	0.44009

Differentially expressed inflammatory genes in alcohol-diet–fed ZFP36L1-sufficient ($L1^{FLX}$) and liver-specific ZFP36L1-deficient ($L1^{LKO}$) mice and control diet–fed ZFP36L1-sufficient ($L1^{FLX}$) and liver-specific ZFP36L1-deficient ($L1^{LKO}$) mice are shown. Bold values depict significant differences.

fold (log2FC), with adjusted $P < 0.05$. Interestingly, although 584 transcripts were significantly differentially expressed (393 up-regulated; 191 down-regulated) in the alcohol diet–fed $L1^{FLX}$ mice compared with control diet–fed $L1^{FLX}$ mice, only 159 transcripts were differentially expressed (92 up-regulated; 67 down-regulated) in the alcohol diet–fed $L1^{LKO}$ mice compared with control diet–fed $L1^{LKO}$ mice (Figure 4, A and B). Fifty transcripts were differentially expressed (26 up-regulated; 24 down-regulated) between alcohol diet–fed $L1^{LKO}$ and alcohol diet–fed $L1^{FLX}$ mice (Figure 4C), whereas only 10 transcripts were differentially expressed (7 up-regulated; 3 down-regulated) between control diet–fed $L1^{LKO}$ and control diet–fed $L1^{FLX}$ mice (Figure 4D). Figure 4E shows a heat map comparing differentially expressed transcripts in the four groups. These data indicate that, in line with the increased steatosis, liver injury, and inflammation seen in the alcohol diet–fed $L1^{FLX}$ mice, there were larger numbers of transcriptomic changes, whereas minimal to no steatosis and significantly attenuated liver injury and inflammation were associated with comparatively lesser numbers of transcriptomic changes in alcohol diet–fed $L1^{LKO}$ mice.

Next, the expression levels of known proinflammatory mRNAs between the two groups were compared to investigate whether the large numbers of gene expression changes in the alcohol diet–fed $L1^{FLX}$ versus alcohol diet–fed $L1^{LKO}$ group could be accounted for by proinflammatory mRNAs. A large proportion of the known inflammatory genes were significantly up-regulated in the $L1^{FLX}$ group (alcohol diet–fed $L1^{FLX}$ mice versus control diet–fed $L1^{FLX}$ mice), but not in the $L1^{LKO}$ group (alcohol diet–fed $L1^{LKO}$ mice versus control diet–fed $L1^{LKO}$ mice) (Table 1). Key inflammatory genes included toll-like 4-receptor *Cd14*, macrophage scavenger receptor, *Marco*, interleukin receptor, *Il3ra*, chemokines including *Ccl2*, *Ccr1, Cxcl2, Cxcl14,* and *Ccrl2,* TNF receptor superfamily proteins, *Tnfrsf10b* and *Tnfrsf21,* NFKB family proteins *Ikbip* and *Nfkbib,* MAP kinase 4 *(Mapk4),* complement component, *C3ar1,* cell surface receptors, *Cd34, Cd68,* and *Cd44,* protein kinase substrate protein, *Marcksl1,* and metalloelastases, *Mmp12* and *Timp*. Interestingly, few of the mRNAs that achieved statistical significance in the alcohol diet–fed $L1^{LKO}$ group were up-regulated by a comparatively lower-fold change when compared with the alcohol diet–fed $L1^{FLX}$ group. Feeding alcohol resulted in significantly increased liver inflammation in $L1^{FLX}$ mice, but not in $L1^{LKO}$ mice.

Comparison of Expression of Alcohol-Regulated Metabolic mRNAs in Alcohol Diet–Fed $L1^{LKO}$ versus the Alcohol Diet–Fed $L1^{FLX}$ Mice

Alcohol ingestion results in metabolic changes including increased lipogenesis, decreased fatty acid oxidation, mobilization of fat from various body deposits into the liver, and impaired very low-density lipoprotein secretion, all resulting in the development of hepatic steatosis.[17] A large number of metabolic genes are involved in this process. To delineate the mechanisms for differential responses of the $L1^{FLX}$ versus the $L1^{LKO}$ mice to alcohol feeding, the RNA-Seq data set was queried for changes in known metabolic transcripts. Sirtuin 1 (*Sirt1*), fatty acid synthase (*Fasn*), stearoyl-coenzyme A desaturase 1 (*Scd*1), acyl-coenzyme A dehydrogenase family member 8 (*Acad8*), and cytochrome P450 family 2 subfamily e polypeptide 1 (*Cyp2e1*) were significantly down-regulated in alcohol diet–fed $L1^{FLX}$ group but were unchanged in the alcohol diet–fed $L1^{LKO}$ group, whereas Lipin-3 and lipoprotein lipase (*Lpl*) were significantly up-regulated in alcohol diet–fed $L1^{FLX}$ group but were unchanged in the alcohol diet–fed $L1^{LKO}$ group. Peroxisome proliferator activated receptor alpha (*Ppara*) and sterol regulatory element binding transcription factor 1

Table 2 Metabolic Genes

Gene symbol	Gene name	$L1^{FLX}$ alcohol diet vs ctrl diet (log2FC)	$L1^{FLX}$ alcohol diet vs ctrl diet (padj)	$L1^{LKO}$ alcohol diet vs ctrl diet (log2FC)	$L1^{LKO}$ alcohol diet vs ctrl diet (padj)
Metabolic regulator genes					
Sirt1	Sirtuin 1	**−0.93**	**0.01**	−0.08	0.88
Sirt3	Sirtuin 3	**−1.32**	**0.02**	**−0.90**	**0.001**
Lipid metabolism					
Lpin1	Lipin 1	**−1.12**	**0.07**	**−1.28**	**0.01**
Lpin2	Lipin 2	−0.31	0.75	**−0.90**	**0.008**
Lpin3	Lipin 3	**1.33**	**0.02**	0.25	0.67
Lpl	Lipoprotein lipase	**2.3**	**0.001**	0.3	0.55
Lipogenesis					
Srebf1	Sterol regulatory element binding transcription factor 1	**−2.28**	**5.99^{-05}**	**−1.68**	**6.15^{-07}**
Fasn	Fatty acid synthase	**−1.78**	**0.05**	−0.64	0.32
Scd1	Stearoyl coenzyme A desaturase 1	**−1.89**	**0.03**	−0.54	0.48
Fatty acid oxidation					
Ppara	Peroxisome proliferator activated receptor alpha	**−1.19**	**0.01**	**−0.98**	**0.04**
Acad8	Acyl-coenzyme A dehydrogenase family member 8	**−0.65**	**0.03**	−0.29	0.36
Cpt1a	Carnitine palmitoyltransferase 1a liver	−0.39	0.71	**−0.94**	**0.01**
Cd36	CD36 antigen	−0.02	0.98	0.27	0.75
Fgf21	Fibroblast growth factor 21	0.7	0.60	**2.0**	**5.92^{-06}**
Alcohol metabolism					
Aldh1a1	Aldehyde dehydrogenase family 1 subfamily A1	−0.75	0.28	0.21	0.68
Cyp2e1	Cytochrome P450 family 2 subfamily e polypeptide 1	**−1.54**	**0.003**	−0.74	0.14

Differentially expressed metabolic genes in alcohol-diet–fed ZFP36L1-sufficient ($L1^{FLX}$) and liver-specific ZFP36L1-deficient ($L1^{LKO}$) mice and control diet–fed ZFP36L1-sufficient ($L1^{FLX}$) and liver-specific ZFP36L1-deficient ($L1^{LKO}$) mice are shown. Bold values depict significant differences.

(*Srebf1*) were significantly down-regulated in both the $L1^{FLX}$ and $L1^{LKO}$ groups following alcohol ingestion, although the fold change was higher in the $L1^{FLX}$ group (Table 2).

FGF21, a Peptide Metabolic Hormone, Is Significantly Increased in the Alcohol Diet–Fed $L1^{LKO}$ Group Compared with the Alcohol Diet–Fed $L1^{FLX}$ Group

FGF21 is known to be up-regulated following alcohol feeding and has been reported to have a protective role in alcoholic steatohepatitis, both in mice and humans.[23,24] RNA-Seq analyses revealed that *Fgf21* was significantly up-regulated by 4.2-fold (Log2FC = 2.0; padj = 5.92^{E06}) in alcohol diet–fed $L1^{LKO}$ mice versus the control diet–fed $L1^{LKO}$ mice but was unchanged in alcohol diet–fed $L1^{FLX}$ mice versus the control diet–fed $L1^{FLX}$ (padj = 0.60) (Table 2). Consistent with the RNA-Seq data, quantitative PCR also indicated significant up-regulation of *Fgf21* mRNA in the alcohol diet–fed $L1^{LKO}$ group (Figure 5A). Next, to test whether secretory levels of FGF21 in the serum were affected in alcohol diet–fed $L1^{LKO}$ mice, an enzyme-linked immunosorbent assay was performed on serum samples collected from alcohol diet–fed and control diet–fed $L1^{FLX}$ and $L1^{LKO}$ mice. The results showed that FGF21 was significantly increased in alcohol diet–fed $L1^{LKO}$ mice, but not in the alcohol diet–fed $L1^{FLX}$ mice (Figure 5B). These data indicated that *Fgf21* may be regulated by ZFP36L1 in this model.

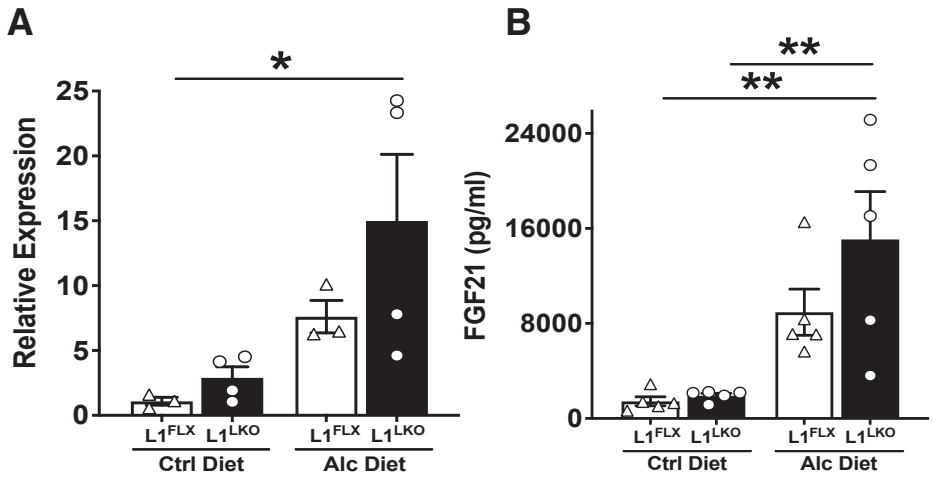

Figure 5 FGF21 is significantly increased in alcohol diet—fed ZFP36L1 LKO mice. **A:** Relative expression of *Fgf21* mRNA in the liver homogenate from alcohol diet—fed ZFP36L1-sufficient ($L1^{FLX}$) and liver-specific ZFP36L1-deficient ($L1^{LKO}$) mice and control diet—fed ZFP36L1-sufficient ($L1^{FLX}$) and liver-specific ZFP36L1-deficient ($L1^{LKO}$) mice. **B:** Secreted levels of FGF21 (picograms per milliliter) in the serum of alcohol diet—fed ZFP36L1-sufficient ($L1^{FLX}$) and liver-specific ZFP36L1-deficient ($L1^{LKO}$) mice, and control diet—fed ZFP36L1-sufficient ($L1^{FLX}$) and liver-specific ZFP36L1-deficient ($L1^{LKO}$) mice. Data are expressed as means ± SEM. $n = 3$ to 4 mice (**A**); $n = 5$ mice (**B**). $^*P < 0.05$, $^{**}P < 0.01$ (one-way analysis of variance followed by Tukey's correction for multiple comparisons). Alc, alcohol; Ctrl, control; FGF21, fibroblast growth factor 21.

ZFP36L1 Regulates *Fgf21* mRNA Turnover through AREs in Its 3′UTR

Because ZFP36 family members regulate their target mRNAs by binding to their 3′UTR AREs,[2] whether *Fgf21* mRNA contains AREs in its 3′UTR and whether those could be potential ZFP36L1 binding sites was investigated. As expected, the 3′UTR of *Fgf21* mRNA contains at least three highly conserved potential ZFP36L1 binding sites (AREs) within its 3′UTR (Figure 6A). Next, to test whether ZFP36L1 regulates *Fgf21* mRNA, the complete 3′UTR of *Fgf21* mRNA was cloned (a total of 163 bp were cloned that also included 37 bp of the protein coding region) into the pMIR-REPORT luciferase reporter construct. Whether ZFP36L1 can regulate the

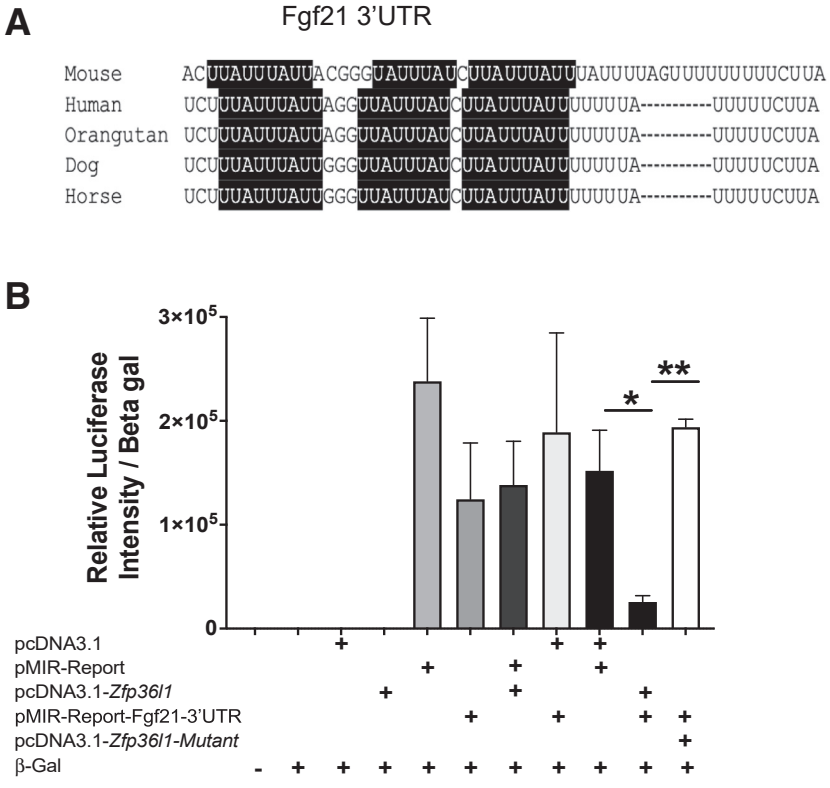

Figure 6 ZFP36L1 regulates the 3′UTR of *Fgf21* mRNA. **A:** At least three evolutionarily conserved AU-rich elements (AREs) are present in the 3′-untranslated region (3′UTR) of the *Fgf21* transcript. The AREs are highlighted in black. **B:** HEK293 cells were transfected with empty vector (pcDNA 3.1), luciferase reporter (pMIR-REPORT), WT-human ZFP36L1 expression plasmid (pcDNA 3.1-*Zfp36l1*), ZFP36L1 expression plasmid with C135R, C173R zinc finger mutation (pcDNA 3.1-*Zfp36l1*-mutant), and pMIR-REPORT vector expressing the 3′UTR of *Fgf21 (*pMIR-REPORT-*Fgf21-3′UTR)* in various combinations. Beta-galactosidase (Beta gal) was transfected as an internal control, and data are represented as relative luciferase activity normalized to beta-galactosidase activity. Bar 1: untransfected; bar 2: beta-galactosidase only; bar 3: pcDNA 3.1 empty vector only; bar 4: pcDNA 3.1-*Zfp36l1-wt*; bar 5; pMIR-REPORT empty vector only; bar 6: pMIR-REPORT-*Fgf21*-3′UTR-reporter; bar 7: pMIR-REPORT empty vector + pcDNA 3.1 *Zfp36l1-wt*; bar 8: pcDNA 3.1 empty vector + pMIR-REPORT *Fgf21*-3′UTR-reporter; bar 9: pcDNA 3.1 empty vector + pMIR-REPORT empty vector; bar 10: pcDNA 3.1 *Zfp36l1-wt* + pMIR-REPORT-*Fgf21*-3′UTR; bar 11: pcDNA 3.1 *Zfp36l1*-mutant + pMIR-REPORT *Fgf21*-3′UTR. Data are expressed as means ± SEM. $n = 3$. $^*P < 0.05$, $^{**}P < 0.01$ (one-way analysis of variance followed by Tukey's correction for multiple comparisons).

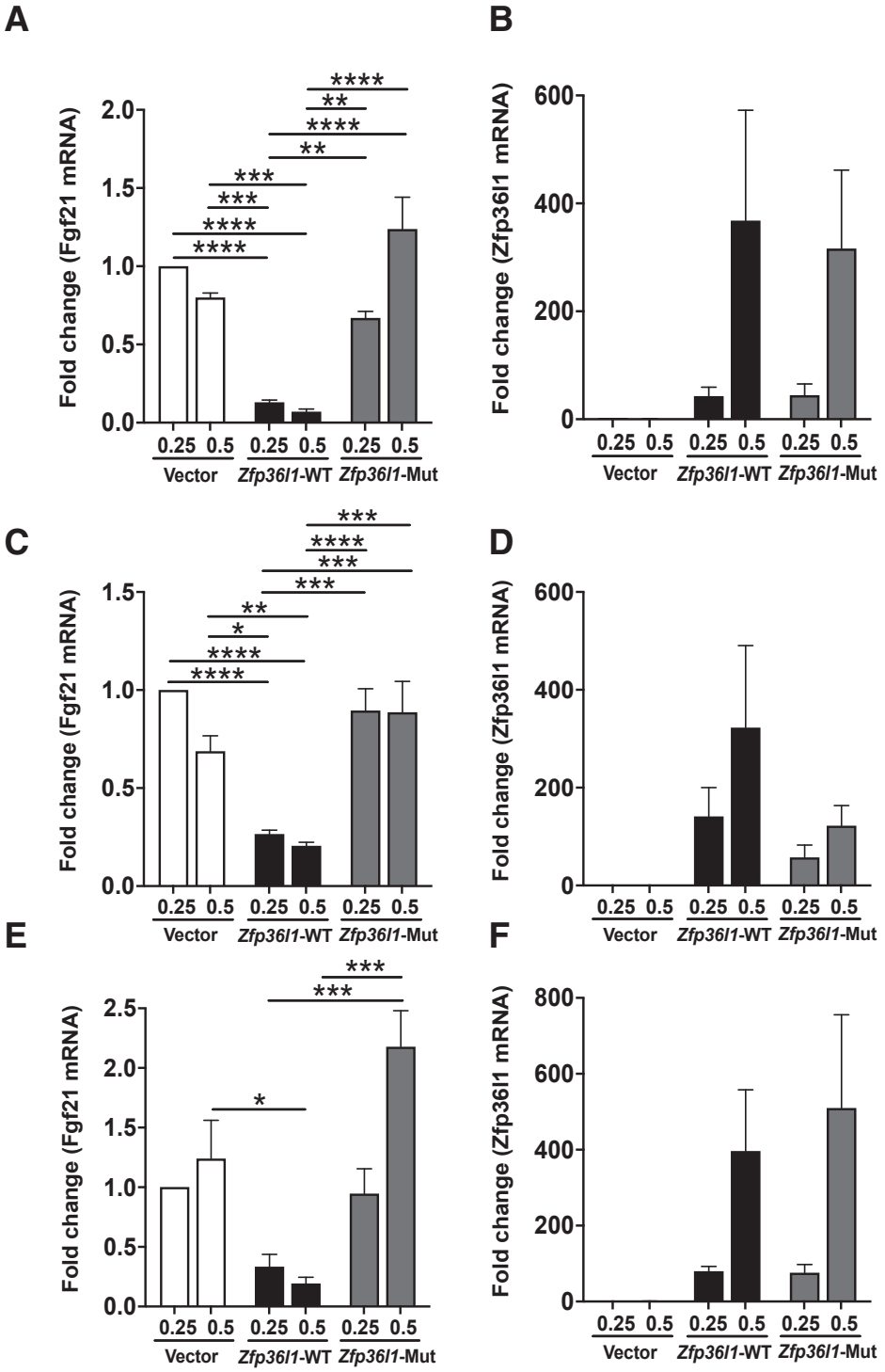

Figure 7 ZFP36L1 reduces the steady state levels of *Fgf21* mRNA. Wild-type *Zfp36l1* or its non-binding mutant (zinc finger mutant) plasmids were cotransfected with plasmid expressing full-length *Fgf21* mRNA in HEK293 cells. **A, C,** and **E:** Relative expression of *Fgf21* mRNA 12 hours (**A**), 24 hours (**C**), and 48 hours (**E**) post-transfection. Bars 1 and 2 show *Fgf21* mRNA expression following the transfection of pcDNA 3.1 empty vector at 0.25 and 0.50 μg, respectively; bars 3 and 4 show *Fgf21* mRNA expression following the transfection of wild-type *Zfp36l1* at 0.25 and 0.50 μg, respectively; and bars 5 and 6 show *Fgf21* mRNA expression following the transfection of zinc finger mutant *Zfp36l1* at 0.25 and 0.50 μg, respectively. **B, D,** and **F:** Relative expression of *Zfp36l1* in HEK293 cells transfected with pcDNA 3.1 empty vector, wild-type *Zfp36l1* expression plasmid, and zinc finger mutant *Zfp36l1* expression plasmid at 12 hours (**B**), 24 hours (**D**), and 48 hours (**F**) post-transfection. Data are expressed as means ± SEM. $n = 4$ independent experiments. $^{*}P < 0.05$, $^{**}P < 0.01$, $^{***}P < 0.001$, and $^{****}P < 0.0001$ (one-way analysis of variance followed by Tukey's correction for multiple comparisons). Mut, mutant; WT, wild-type.

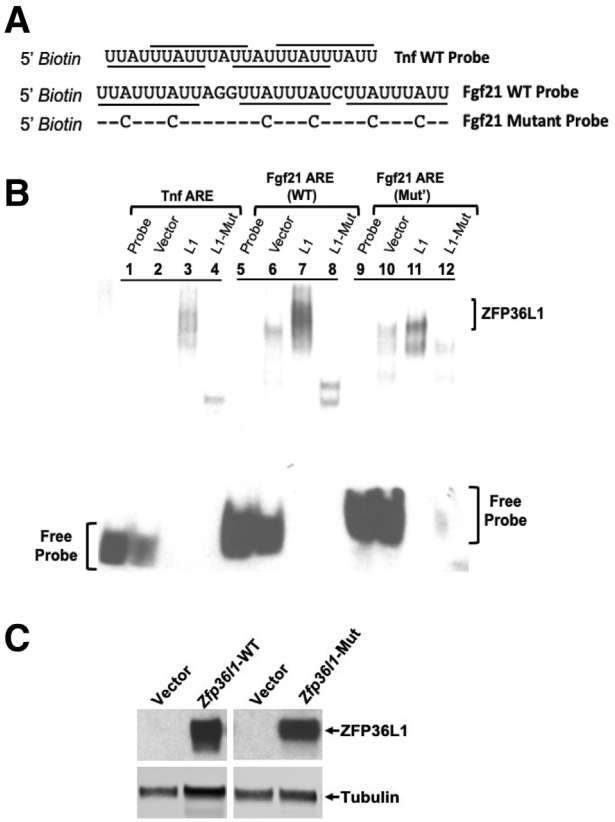

Figure 8 ZFP36L1 binds to the ARE from *Fgf21* mRNA in electrophoretic mobility shift assay. RNA electrophoretic gel-shift mobility assay with ZFP36L1-WT, ZFP36L1-mutant, WT-*Fgf21*-ARE, and Mutant-*Fgf21*-ARE. **A:** Sequences of 5′-biotin—labelled RNA probes corresponding to the WT *Tnf* ARE (*https://www.ncbi.nlm.nih.gov/nuccore/X02611*; accession number X02611), WT *Fgf21* ARE (*https://www.ncbi.nlm.nih.gov/nuccore/NM_019113.4*; accession number NM_019113.4), and mutant human *Fgf21* ARE in which six A residues were replaced by C residues. The ARE binding sites (octamer and nonamers) are **underlined**. The **hyphens** indicate the sequence identify at that position to the WT-*Fgf21* ARE probe. **B:** HEK293 cells were transfected with vector alone (pcDNA 3.1), WT-human ZFP36L1 expression construct (pcDNA 3.1-*Zfp36l1*), or the human ZFP36L1 expression construct with C135R, C173R zinc finger mutation (pcDNA 3.1-*Zfp36l1*-mutant). Equal amounts of these cytosolic extracts were combined with a probe derived from *Tnf* ARE (lanes 1 to 4), WT-*Fgf21* ARE (lanes 5 to 8), and Mutant-*Fgf21* ARE (lanes 9 to 12), and gel-shift assay was performed. Lanes 1 and 2 show the position of the free *Tnf* probe when either free probe only (lane 1) was used or the probe was combined with empty vector-expressing lysates (lane 2). A large complex was formed with the WT-ZFP36L1 (lane 3), but not with the mutant-ZFP36L1 (lane 4). Lanes 5 (probe alone) and 6 (probe with empty vector) show the position of the free *Fgf21*-WT probe. The amount of probe and the migration position of the complex formed were shifted with WT-ZFP36L1 (lane 7), but not with the mutant-ZFP36L1 (lane 8). Lanes 9 (probe alone) and 10 (probe with empty vector) show the position of the free *Fgf21*-mutant probe. The amount of probe and the migration positions of the complex formed were partially shifted with WT-ZFP36L1 (lane 11), but not with the mutant-ZFP36L1 (lane 12). **C:** Immunoblot of the cytosolic extracts from cells transfected with vector (pcDNA 3.1) alone, wild-type human ZFP36L1, or the zinc finger mutant (C135R, C173R) form of ZFP36L1 that were used in the RNA electrophoretic mobility shift assay. The position of ZFP36L1 is indicated to the right. The **bottom gels** show the loading control, tubulin. ARE, AU-rich element; Mut, mutant; WT, wild-type.

stability of *Fgf21* mRNA 3′UTR in luciferase reporter assays was tested. As shown in Figure 6B, the untransfected control (bar 1) or the transfection of beta-galactosidase alone (bar 2) did not result in detectable luciferase activity/luminescence. Similarly, transfection of an empty pcDNA3.1 vector alone (bar 3) or a plasmid expressing WT ZFP36L1 (pcDNA3.1-*Zfp36l1*) did not result in detectable luciferase activity. Luciferase activity was reported from cells transfected with the pMIR-REPORT (luciferase reporter expression vector) (bar 5), the pMIR-REPORT containing *Fgf21*-3′UTR (bar 6), a combination of pMIR-REPORT and pcDNA3.1 plasmid expressing WT ZFP36L1 (bar 7), a combination of pMIR-REPORT expressing *Fgf21*-3′UTR and pcDNA 3.1 empty vector (bar 8), and a combination of two empty plasmids (pMIR-REPORT + pcDNA 3.1) (bar 9). Luciferase activity was significantly inhibited (bar 10) when WT ZFP36L1 and the pMIR-*Fgf21*-3′UTR were present together, indicating that ZFP36L1 decreased the stability of *Fgf21*-3′UTR. In comparison to this, the luciferase activity was significantly rescued when the ZFP36L1 zinc finger mutant (C135R, C173R) was present (bar 11), indicating that the two intact zinc fingers are essentially required for this effect. These data show that ZFP36L1 directly regulates *Fgf21*-3′UTR and that this effect is mediated through the two zinc finger domains of ZFP36L1

ZFP36L1 Promotes the Decay of Full-Length *Fgf21* mRNA via the Zinc Finger Motif

The ability of ZFP36L1 to destabilize a full-length transcript of *Fgf21* through cotransfection assays in HEK293 cells was tested next. When a full-length *Fgf21*-mRNA was coexpressed with ZFP36L1-WT protein, the steady-state levels of *Fgf21* mRNA were decreased at both 0.25 μg and 0.5 μg concentrations of ZFP36L1 (Figure 7, A, C, and E). This effect was statistically significant at both 12 and 24 hours for 0.5 and 0.25 μg (Figure 7, A and C) and at 48 hours for 0.5 μg (Figure 7E). However, when a full-length *Fgf21*-mRNA was coexpressed with zinc finger ZFP36L1-mutant (C135R, C173R), the levels of *Fgf21* mRNA did not decrease at either the low (0.25 μg) or the high (0.5 μg) concentration of ZFP36L1-mutant plasmid (Figure 7, A, C, and E). Figures 7, B, D, and F show the dose-dependent increase in the expression of ZFP36L1-WT and ZFP36L1-mutant in this experiment at 12 (Figure 7B), 24 (Figure 7D), and 48 (Figure 7F) hours, respectively. This assay suggested that ZFP36L1 promotes the decay of *Fgf21* mRNA and that the zinc finger motif of ZFP36L1 is required for this effect.

ZFP36L1 Binds to *Fgf21*-mRNA 3′UTR AU-Rich Region

Finally, whether ZFP36L1 expressed in HEK293 cells can directly bind to AREs within the 3′UTR of *Fgf21* mRNA was tested. Biotin 5′-end—labelled RNA probes designed from the 3′UTR of *Fgf21* mRNA were synthesized. The

probes consisted of a WT *Fgf21*-ARE and a mutant *Fgf21*-ARE in which all the six core A residues were mutated to C residues (Figure 8A). Mutation of core A residues to C residues has been previously shown to abrogate the binding of TTP to its target mRNA probes.[25] A *Tnf* 3′UTR-ARE probe was used as a positive control. Cell lysates expressing WT ZFP36L1 or zinc finger mutant ZFP36L1 (C135R, C173R) were incubated with WT *Tnf*, WT *Fgf21*, or mutated-*Fgf21* mRNA ARE probes, and RNA mobility shift assays were performed. As shown in Figure 8B, cytosolic extracts from cells expressing vector alone (lane 2) did not bind *Tnf*-ARE. The migration position of the free probe is depicted in lane 1. *Tnf*-ARE was able to bind to ZFP36L1, as is evident from the slower migration of the probe (lane 3). The *Tnf*-ARE probe was also able to bind to a small amount of zinc finger mutant-ZFP36L1, but with greatly reduced ability (lane 4) compared with WT ZFP36L1 (lane 3), as is evident from the increased migration (downward shifting of the band) in this case (lane 4). When the WT *Fgf21*-ARE probe was used, significant binding was evident with the WT ZFP36L1 protein (lane 7). The bound *Fgf21*-ZFP36L1 complex exhibited significantly reduced migration in the gel, indicating good binding. The binding also appeared to be much better than was observed with the *Tnf*-ARE, as is evident from the larger size and increased intensity of the band (lane 7). Again, the zinc finger mutant-ZFP36L1 was still able to bind the WT *Fgf21*-ARE but with markedly reduced ability (lane 8). The position of the WT *Fgf21*-ARE free probe is shown in lane 5. Lane 6 shows the vector control. Finally, as shown in lane 11, the mutant-*Fgf21*-ARE probe was able to bind to the WT ZFP36L1 protein; however, its ability to bind was much less than that of the WT *Fgf21*-ARE probe (lane 7). This is clear from increased migration (downward shifting of the band) and reduced intensity and splitting of the band (lane 11). The mutant-*Fgf21*-ARE probe was, however, not able to bind to the mutant-ZFP36L1 (lane 12). The position of the mutant-*Fgf21*-ARE free probe is shown in lane 9. Lane 10 shows the vector control. Figure 8C shows equivalent expression of WT and mutated ZFP36L1 in HEK293 cells.

Discussion

Excessive alcohol consumption is a global problem with enormous clinical and economic consequences.[26] Liver, the primary site of alcohol metabolism, sustains the greatest tissue injury following alcohol ingestion. However, the pathogenic mechanisms involved in alcoholic hepatic steatosis, injury, and inflammation remain incompletely understood. The current study describes an interesting role of a post-transcriptional regulator of gene expression, that is, ZFP36L1, in the pathogenesis of alcohol-induced changes in the liver.

Liver-specific ablation of ZFP36L1 ($L1^{LKO}$ mice) resulted in significant reduction in hepatic steatosis, liver injury, and inflammation in response to alcohol when compared with mice that contained an intact *Zfp36l1* gene ($L1^{FLX}$ mice). These findings suggest that ZFP36L1 promotes instability of mRNAs that confer protection against alcohol-induced liver injury. Along similar lines, liver-specific loss of ZFP36L1 was shown to confer protection against diet-induced obesity and steatosis by altering bile acid metabolism through regulation of cholesterol 7α−hydroxylase (Cyp7a1) mRNA.[11] Loss of ZFP36L1 was also shown to protect against the development of experimental osteoarthritis through the post-transcriptional regulation of heat shock protein 70 family members.[27] Finally, a recent study showed that ZFP36L1 is required for the maintenance of the marginal zone B-cell compartment, and this effect is dependent on its regulation of the transcription factors KLF2 and IRF8.[28] Together, these studies indicate that ZFP36L1 regulates a variety of physiological and pathological responses through its mRNA targets.

Alcoholic hepatitis is a serious consequence of alcoholic liver disease and is accompanied by increased expression of proinflammatory mediators that recruit inflammatory cells into the liver. RNA-sequencing revealed that a large number of inflammatory mRNAs were significantly up-regulated in $L1^{FLX}$ mice, but not in the $L1^{LKO}$ mice, after alcohol administration. For instance, TNFα levels are increased in both human alcoholic liver and in animal models of liver disease.[29] *Tnf* mRNA was significantly up-regulated in $L1^{FLX}$, but not in the $L1^{LKO}$ group, after alcohol challenge. MCP1, also known as CCL2, levels are increased in the plasma of patients with alcoholic liver disease and have been correlated with liver neutrophil infiltrates after alcohol.[30] Further, deficiency of MCP1 has been shown to protect against alcoholic liver injury.[19] *Mcp1/Ccl2* was significantly up-regulated in the $L1^{FLX}$, but not in the $L1^{LKO}$ mice, after alcohol administration. *Cd14* (a coreceptor for toll-like receptor 4) was specifically up-regulated in the alcohol diet−fed $L1^{FLX}$ group but was unchanged in the alcohol diet−fed $L1^{LKO}$ group. CD14-deficient mice have been shown to exhibit reduced early alcohol-induced liver injury.[31] Liver macrophages and monocytes from alcoholic hepatitis patients show increased activation of NFκB.[32] *Ikbip* and *Nfkbib*, two members of NFκB family, were significantly up-regulated in the alcohol diet−fed $L1^{FLX}$ group but were unchanged in the alcohol diet−fed $L1^{LKO}$ group. Similarly, *Mapk4,* a member of the MAP kinase signaling family, is up-regulated following alcohol exposure, both *in vitro* and *in vivo*.[32] Although *Mapk4* was significantly up-regulated in the alcohol diet−fed $L1^{FLX}$ group, its expression levels remained unchanged in the alcohol diet−fed $L1^{LKO}$ group. Finally, *Mmp12,* a metalloprotease involved in extracellular remodeling,[33] was significantly up-regulated in the alcohol diet−fed $L1^{FLX}$ group, but not in the alcohol diet−fed $L1^{LKO}$ group. Of note, *Mmp12* has been shown to be up-regulated in primary murine macrophages following alcohol exposure.[34] These outcomes suggest that the ZFP36L1-deficient liver cells in

alcohol-challenged $L1^{LKO}$ mice exhibit mitigated cellular injury that in turn prevents the pronounced inflammation, a response evident in alcohol-challenged $L1^{FLX}$ mice. Second, we speculate that other members of this protein family, particularly ZFP36/TTP, can regulate inflammation, whereas ZFP36L1 regulates metabolic genes within the liver. These possibilities, however, need to be tested further.

FGF21, a liver-specific metabolic hormone, is known to be elevated in the blood of both mice and humans after acute or binge alcohol ingestion.[23,35] Interestingly, FGF21 was significantly up-regulated in the alcohol diet–fed $L1^{LKO}$ group, but not in the alcohol diet–fed $L1^{FLX}$ group, suggesting that ZFP36L1 directly or indirectly regulates the expression of *Fgf21*. This was also indicated by the finding that PPARα, the transcriptional regulator of FGF21, was significantly down-regulated in both the alcohol diet–fed $L1^{FLX}$ and the $L1^{LKO}$ groups. Accordingly, further experiments were conducted to determine whether *Fgf21* is a direct target of ZFP36L1. First, luciferase activity assays were used to demonstrate that ZFP36L1 can destabilize *Fgf21*-3′UTR. Second, cotransfection assays were used to demonstrate that ZFP36L1 can destabilize the full-length *Fgf21* mRNA. Third, electrophoretic mobility shift assays were used to demonstrate that ZFP36L1 can directly bind to the 3′UTR ARE region of *Fgf21* mRNA. Finally, this effect was shown to be mediated by the two tandem zinc finger domains of ZFP36L1, as indicated by the reappearance of the luciferase activity and the stabilization of *Fgf21* mRNA when a zinc finger mutant of ZFP36L1 replaced the WT-ZFP36L1 in the luciferase experiment and the co-expression assays, respectively. These experiments demonstrated that *Fgf21* mRNA can be a target of ZFP36L1.

FGF21 has been previously shown to be a target of ZFP36/TTP, another member of the ZFP36 family of RNA binding proteins. For instance, Sawicki et al[36] demonstrated that *Fgf21* mRNA is post-transcriptionally regulated by ZFP36/TTP, and that liver-specific loss of ZFP36/TTP improves systemic glucose tolerance and insulin sensitivity in mice fed a high-fat diet by up-regulating FGF21. Another study recently demonstrated that CCR4-NOT deadenylase-ZFP36/TTP complex promotes degradation of *Fgf21* mRNA, and that ablation of CCR4-NOT deadenylase activity decreases the susceptibility of mice to metabolic disorders, including obesity and steatosis, by increasing FGF21 levels.[37] The current data provide evidence of redundancy between ZFP36/TTP and ZFP36L1 in the post-transcriptional regulation of *Fgf21* mRNA. However, the relative contribution of ZFP36/TTP versus ZFP36L1 in the post-transcriptional regulation of *Fgf21* mRNA remains unexplored and warrants further investigation.

FGF21 has been shown to confer protection from alcohol-induced hepatic steatosis and liver injury in previous studies. In fact, chronic alcohol feeding in the absence of FGF21 results in significant liver injury in mice.[23] Mice lacking FGF21 have been shown to exhibit exacerbated alcohol-induced liver steatosis and liver injury through activation of genes involved in lipogenesis and repression of genes involved in beta oxidation of fatty acids.[24] Conversely, administration of recombinant FGF21 to WT mice that were chronically fed alcohol was shown to significantly attenuate hepatic steatosis and liver injury.[24] Consistent with these reports, up-regulation of FGF21 was shown to align with the hepatoprotective effect in ZFP36L1 liver-specific knockout mice. However, whether the hepatoprotective effect of ZFP36L1 deletion is mediated through the up-regulated expression of FGF21 alone or through the up-regulation and down-regulation of a battery of anti-inflammatory and proinflammatory genes, respectively, remains to be tested.

Previous studies with the ZFP36 RNA binding protein family have suggested that a number of mRNA targets of these proteins are cell-specific. For instance, *Tnf* has been identified as a myeloid-cell–specific target of ZFP36/TTP.[38] Similarly, *Notch 1* was identified as a thymocyte-specific target of both ZFP36L1 and ZFP36L2.[39] The current study indicates that *Fgf21* mRNA is a target of ZFP36L1 in hepatocytes/cholangiocytes. However, it remains unclear whether this relationship is specific to one or both the cell types. Further, whether the deletion of ZFP36L1 in other cell types such as immune cells and hepatic stellate cells within the liver will also result in the up-regulation of *Fgf21* also warrants further investigation.

Previous studies with ZFP36 RNA binding protein family have also indicated stimulus specificity for their mRNA targets. For example, myeloid-specific loss of ZFP36/TTP did not result in any abnormalities under basal conditions.[40] However, these mice were hypersensitive to lipopolysaccharide challenge that resulted from the stabilization and several-fold up-regulation of the ZFP36/TTP target, *Tnf*.[40] Similarly, TTP deletion in keratinocytes resulted in hypersensitivity to imiquimod-induced skin inflammation in these mice, and this effect was mediated by keratinocyte-specific stabilization and up-regulation of *Tnf*.[41] In a recent study, genetic ablation or silencing of ZFP36L1 significantly protected mice from experimental osteoarthritis by stabilizing members of the heat shock protein 70 family, again indicating stimulus-specific targets and resulting in pathological outcomes.[27] Along these lines, *Fgf21* also appears to be a stimulus-specific physiologically relevant target of ZFP36L1.

Collectively, the current study reveals a novel post-transcriptional mechanism of regulation of FGF21 production during alcohol-induced hepatic disease. First, ZFP36L1 deletion in the liver resulted in significant reductions in hepatic steatosis, liver injury, and inflammation in response to alcohol. Second, biochemical studies demonstrated that ZFP36L1 regulates the expression of FGF21, following basic mechanism through which TTP family members operate to regulate their target mRNAs. Of note, FGF21 is considered as a potential treatment of metabolic disease; therefore, various FGF21 analogs have been developed and

are undergoing clinical trials for metabolic disorders, including diabetes and obesity.[42] The current study suggests that the hepatic ZFP36L1-FGF21 axis is a major signaling route in alcohol-induced hepatic steatosis in mice. This opens up the possibility of silencing ZFP36L1 as a possible method of protection against alcoholic-liver disease.

Acknowledgment

We thank Sherry Ring for histologic tissue processing.

Author Contributions

S.P. conceived and designed the study; S.P. and C.S.B. maintained the animal colony. C.S.B. genotyped the animals and performed all the experiments except those listed further. C.S.B. and J.C. performed the luciferase assays. J.C. performed the cotransfection and the electrophoretic mobility shift assays. Y.S. performed the oral gavages. R.K. performed the Oil Red O staining, the immunohistochemisty, and the liver triglyceride assays. P.J.B. provided the *Zfp36l1* floxed mice and edited the manuscript; S.P. performed the histopathological studies; S.P. and Y.S. wrote and reviewed the manuscript for intellectual content.

Supplemental Data

Supplemental material for this article can be found at *http://doi.org/10.1016/j.ajpath.2021.10.017*.

References

1. Wells ML, Perera L, Blackshear PJ: An ancient family of RNA-binding proteins: still important! Trends Biochem Sci 2017, 42: 285−296
2. Fu M, Blackshear PJ: RNA-binding proteins in immune regulation: a focus on CCCH zinc finger proteins. Nat Rev Immunol 2017, 17: 130−143
3. Stumpo DJ, Broxmeyer HE, Ward T, Cooper S, Hangoc G, Chung YJ, Shelley WC, Richfield EK, Ray MK, Yoder MC, Aplan PD, Blackshear PJ: Targeted disruption of Zfp36l2, encoding a CCCH tandem zinc finger RNA-binding protein, results in defective hematopoiesis. Blood 2009, 114:2401−2410
4. Stumpo DJ, Byrd NA, Phillips RS, Ghosh S, Maronpot RR, Castranio T, Meyers EN, Mishina Y, Blackshear PJ: Chorioallantoic fusion defects and embryonic lethality resulting from disruption of Zfp36L1, a gene encoding a CCCH tandem zinc finger protein of the Tristetraprolin family. Mol Cell Biol 2004, 24:6445−6455
5. Taylor GA, Carballo E, Lee DM, Lai WS, Thompson MJ, Patel DD, Schenkman DI, Gilkeson GS, Broxmeyer HE, Haynes BF, Blackshear PJ: A pathogenetic role for TNF alpha in the syndrome of cachexia, arthritis, and autoimmunity resulting from tristetraprolin (TTP) deficiency. Immunity 1996, 4:445−454
6. Stumpo DJ, Trempus CS, Tucker CJ, Huang W, Li L, Kluckman K, Bortner DM, Blackshear PJ: Deficiency of the placenta- and yolk sac-specific tristetraprolin family member ZFP36L3 identifies likely mRNA targets and an unexpected link to placental iron metabolism. Development 2016, 143:1424−1433
7. Patial S, Curtis AD 2nd, Lai WS, Stumpo DJ, Hill GD, Flake GP, Mannie MD, Blackshear PJ: Enhanced stability of tristetraprolin mRNA protects mice against immune-mediated inflammatory pathologies. Proc Natl Acad Sci U S A 2016, 113:1865−1870
8. Patial S, Blackshear PJ: Tristetraprolin as a therapeutic target in inflammatory disease. Trends Pharmacol Sci 2016, 37:811−821
9. Adachi S, Homoto M, Tanaka R, Hioki Y, Murakami H, Suga H, Matsumoto M, Nakayama KI, Hatta T, Iemura S, Natsume T: ZFP36L1 and ZFP36L2 control LDLR mRNA stability via the ERK-RSK pathway. Nucleic Acids Res 2014, 42:10037−10049
10. Takahashi A, Adachi S, Morita M, Tokumasu M, Natsume T, Suzuki T, Yamamoto T: Post-transcriptional stabilization of Ucp1 mRNA protects mice from diet-induced obesity. Cell Rep 2015, 13: 2756−2767
11. Tarling EJ, Clifford BL, Cheng J, Morand P, Cheng A, Lester E, Sallam T, Turner M, de Aguiar Vallim TQ: RNA-binding protein ZFP36L1 maintains posttranscriptional regulation of bile acid metabolism. J Clin Invest 2017, 127:3741−3754
12. Mu X, Pradere JP, Affo S, Dapito DH, Friedman R, Lefkovitch JH, Schwabe RF: Epithelial transforming growth factor-beta signaling does not contribute to liver fibrosis but protects mice from cholangiocarcinoma. Gastroenterology 2016, 150:720−733
13. Bertola A, Mathews S, Ki SH, Wang H, Gao B: Mouse model of chronic and binge ethanol feeding (the NIAAA model). Nat Protoc 2013, 8:627−637
14. Postic C, Shiota M, Niswender KD, Jetton TL, Chen Y, Moates JM, Shelton KD, Lindner J, Cherrington AD, Magnuson MA: Dual roles for glucokinase in glucose homeostasis as determined by liver and pancreatic beta cell-specific gene knock-outs using Cre recombinase. J Biol Chem 1999, 274:305−315
15. Committee for the Update of the Guide for the Care and Use of Laboratory Animals; National Research Council: Guide for the Care and Use of Laboratory Animals. Eighth Edition. Washington, DC, National Academies Press, 2011
16. Homeyer A, Nasr P, Engel C, Kechagias S, Lundberg P, Ekstedt M, Kost H, Weiss N, Palmer T, Hahn HK, Treanor D, Lundstrom C: Automated quantification of steatosis: agreement with stereological point counting. Diagn Pathol 2017, 12:80
17. Osna NA, Donohue TM Jr, Kharbanda KK: Alcoholic liver disease: pathogenesis and current management. Alcohol Res 2017, 38:147−161
18. Sakhuja P: Pathology of alcoholic liver disease, can it be differentiated from nonalcoholic steatohepatitis? World J Gastroenterol 2014, 20:16474−16479
19. Mandrekar P, Ambade A, Lim A, Szabo G, Catalano D: An essential role for monocyte chemoattractant protein-1 in alcoholic liver injury: regulation of proinflammatory cytokines and hepatic steatosis in mice. Hepatology 2011, 54:2185−2197
20. Thakur V, Pritchard MT, McMullen MR, Wang Q, Nagy LE: Chronic ethanol feeding increases activation of NADPH oxidase by lipopolysaccharide in rat Kupffer cells: role of increased reactive oxygen in LPS-stimulated ERK1/2 activation and TNF-alpha production. J Leukoc Biol 2006, 79:1348−1356
21. Gao B: Hepatoprotective and anti-inflammatory cytokines in alcoholic liver disease. J Gastroenterol Hepatol 2012, 27(Suppl 2):89−93
22. Clugston RD, Jiang H, Lee MX, Piantedosi R, Yuen JJ, Ramakrishnan R, Lewis MJ, Gottesman ME, Huang LS, Goldberg IJ, Berk PD, Blaner WS: Altered hepatic lipid metabolism in C57BL/6 mice fed alcohol: a targeted lipidomic and gene expression study. J Lipid Res 2011, 52:2021−2031
23. Desai BN, Singhal G, Watanabe M, Stevanovic D, Lundasen T, Fisher FM, Mather ML, Vardeh HG, Douris N, Adams AC, Nasser IA, FitzGerald GA, Flier JS, Skarke C, Maratos-Flier E: Fibroblast growth factor 21 (FGF21) is robustly induced by ethanol and has a protective role in ethanol associated liver injury. Mol Metab 2017, 6:1395−1406
24. Liu Y, Zhao C, Xiao J, Liu L, Zhang M, Wang C, Wu G, Zheng MH, Xu LM, Chen YP, Mohammadi M, Chen SY, Cave M, McClain C,

Li X, Feng W: Fibroblast growth factor 21 deficiency exacerbates chronic alcohol-induced hepatic steatosis and injury. Sci Rep 2016, 6: 31026
25. Lai WS, Carrick DM, Blackshear PJ: Influence of nonameric AU-rich tristetraprolin-binding sites on mRNA deadenylation and turnover. J Biol Chem 2005, 280:34365−34377
26. Bouchery EE, Harwood HJ, Sacks JJ, Simon CJ, Brewer RD: Economic costs of excessive alcohol consumption in the U.S., 2006. Am J Prev Med 2011, 41:516−524
27. Son YO, Kim HE, Choi WS, Chun CH, Chun JS: RNA-binding protein ZFP36L1 regulates osteoarthritis by modulating members of the heat shock protein 70 family. Nat Commun 2019, 10:77
28. Newman R, Ahlfors H, Saveliev A, Galloway A, Hodson DJ, Williams R, Besra GS, Cook CN, Cunningham AF, Bell SE, Turner M: Maintenance of the marginal-zone B cell compartment specifically requires the RNA-binding protein ZFP36L1. Nat Immunol 2017, 18:683−693
29. McClain CJ, Barve S, Barve S, Deaciuc I, Hill DB: Tumor necrosis factor and alcoholic liver disease. Alcohol Clin Exp Res 1998, 22: 248S−252S
30. Degre D, Lemmers A, Gustot T, Ouziel R, Trepo E, Demetter P, Verset L, Quertinmont E, Vercruysse V, Le Moine O, Deviere J, Moreno C: Hepatic expression of CCL2 in alcoholic liver disease is associated with disease severity and neutrophil infiltrates. Clin Exp Immunol 2012, 169:302−310
31. Yin M, Bradford BU, Wheeler MD, Uesugi T, Froh M, Goyert SM, Thurman RG: Reduced early alcohol-induced liver injury in CD14-deficient mice. J Immunol 2001, 166:4737−4742
32. Mandrekar P, Szabo G: Signalling pathways in alcohol-induced liver inflammation. J Hepatol 2009, 50:1258−1266
33. Duarte S, Baber J, Fujii T, Coito AJ: Matrix metalloproteinases in liver injury, repair and fibrosis. Matrix Biol 2015, 44-46: 147−156
34. Kim MJ, Nepal S, Lee ES, Jeong TC, Kim SH, Park PH: Ethanol increases matrix metalloproteinase-12 expression via NADPH oxidase-dependent ROS production in macrophages. Toxicol Appl Pharmacol 2013, 273:77−89
35. Soberg S, Andersen ES, Dalsgaard NB, Jarlhelt I, Hansen NL, Hoffmann N, Vilsboll T, Chenchar A, Jensen M, Grevengoed TJ, Trammell SAJ, Knop FK, Gillum MP: FGF21, a liver hormone that inhibits alcohol intake in mice, increases in human circulation after acute alcohol ingestion and sustained binge drinking at Oktoberfest. Mol Metab 2018, 11:96−103
36. Sawicki KT, Chang HC, Shapiro JS, Bayeva M, De Jesus A, Finck BN, Wertheim JA, Blackshear PJ, Ardehali H: Hepatic tristetraprolin promotes insulin resistance through RNA destabilization of FGF21. JCI Insight 2018, 3:e95948
37. Morita M, Siddiqui N, Katsumura S, Rouya C, Larsson O, Nagashima T, Hekmatnejad B, Takahashi A, Kiyonari H, Zang M, St-Arnaud R, Oike Y, Giguere V, Topisirovic I, Okada-Hatakeyama M, Yamamoto T, Sonenberg N: Hepatic posttranscriptional network comprised of CCR4-NOT deadenylase and FGF21 maintains systemic metabolic homeostasis. Proc Natl Acad Sci U S A 2019, 116: 7973−7981
38. Carballo E, Lai WS, Blackshear PJ: Feedback inhibition of macrophage tumor necrosis factor-alpha production by tristetraprolin. Science 1998, 281:1001−1005
39. Hodson DJ, Janas ML, Galloway A, Bell SE, Andrews S, Li CM, Pannell R, Siebel CW, MacDonald HR, De Keersmaecker K, Ferrando AA, Grutz G, Turner M: Deletion of the RNA-binding proteins ZFP36L1 and ZFP36L2 leads to perturbed thymic development and T lymphoblastic leukemia. Nat Immunol 2010, 11:717−724
40. Qiu LQ, Stumpo DJ, Blackshear PJ: Myeloid-specific tristetraprolin deficiency in mice results in extreme lipopolysaccharide sensitivity in an otherwise minimal phenotype. J Immunol 2012, 188: 5150−5159
41. Andrianne M, Assabban A, La C, Mogilenko D, Salle DS, Fleury S, Doumont G, Van Simaeys G, Nedospasov SA, Blackshear PJ, Dombrowicz D, Goriely S, Van Maele L: Tristetraprolin expression by keratinocytes controls local and systemic inflammation. JCI Insight 2017, 2:e92979
42. Struik D, Dommerholt MB, Jonker JW: Fibroblast growth factors in control of lipid metabolism: from biological function to clinical application. Curr Opin Lipidol 2019, 30:235−243